Anharmonic Properties of Semiconductors from Density-Functional Perturbation Theory

Thesis submitted for the degree of

"Doctor Philosophiæ"

CANDIDATE

Alberto Debernardi

SUPERVISOR

Prof. Stefano Baroni

October 1995

Ai miei genitori

Chiara e Luigi

Table of Contents

1 Introduction

One of the achievements of solid state physics in this century is the understanding of the vibrational properties of crystals. In fact, the assumption of a static lattice with atoms at their equilibrium positions is an oversimplification that can be used only in specific cases. To obtain a correct theoretical description of many physical properties we must allow the atoms to vibrate around their equilibrium positions. For example, the temperature dependence of the specific heat can be predicted only by including lattice vibrations. If the atomic vibrations have a small amplitude compared to the interatomic distance, it is convenient to expand the energy in powers of the displacements of the atoms from their equilibrium positions, and retain only terms up to second order. In this case we have to solve a harmonic problem.

Information on the phonon dispersion can be obtained experimentally by allowing some external probe to exchange energy with the lattice. Such a probe can consist of photons of visible light (usually from a high intensity laser beam) which are then scattered with absorption or emission of phonons. The change in the photon energy is small, but it can be measured, usually with diffraction grating spectrometers. This process is called Raman scattering when the phonon absorbed or emitted is optical, Brillouin scattering when it is acoustic. Light scattering gives information only about phonons with very small wavevectors. Also neutrons can be used to provide information on phonon branches. Although the neutron data are less accurate than those obtained by Raman spectroscopy, neutron scattering gives information on the normal-mode dispersion relation throughout the Brillouin zone.

In some cases retaining only second order terms in the energy expansion is not suf-

ficient, and higher order corrections must be included. For instance, a harmonic crystal does not present thermal expansion. This is clearly an unphysical feature, because we experimentally observe that the volume of a crystal depends on temperature. This is due to the fact that, if we the neglect anharmonic effects, the phonon frequencies do not depend on volume nor on temperature. The dependence of the phonon frequencies on the crystal volume is described by the so called Grüneisen parameters which measure the importance of anharmonic effects. By including them, it is therefore possible to predict the thermal-expansion coefficient.

Another interesting physical property due to anharmonicity is the phonon lifetime. In a perfect harmonic crystal, phonons do not interact with each other, so that a non equilibrium phonon population would persist in time. However, one experimentally observes that the phonon population decays towards equilibrium on a time scale of a few picoseconds. The anharmonic decay of phonons into vibrations of lower frequency is a fundamental mechanism for energy relaxation in semiconductors, as it controls the formation and time-evolution of the non-equilibrium phonon populations which are emitted by high-density excited carriers when they decay towards their ground state [1]. Many technologically important processes in which electrons are excited high into the conduction band—either optically or by an applied electric field—can be influenced by the presence of hot phonons because these can be reabsorbed by electrons, thus leading to a much slower relaxation of the whole system towards equilibrium.

Experimentally, anharmonic lifetimes of individual zone-center phonons can be extracted from their measured Raman linewidths, if inhomogeneous broadening effects can be neglected. Menéndez and Cardona have obtained the full temperature dependence for elemental semiconductors more than a decade ago [2]. This task is however much more difficult in systems, such as heterostructures, where composition and/or strain inhomogeneities add to the usual (e.g. isotopic [3]) broadening factors. Experiments in the time domain by ultrafast spectroscopies have also become available in recent years, but their interpretation is often not straightforward, especially in complex structures, owing to the coupling between the dynamics of carrier and phonon populations [1].

The anharmonic decay of phonons in semiconductors is the main subject of this thesis. In Chapter 2 we introduce the phonon lifetime both from an experimental and a theo-

retical points of view, and we review the previous attempts to compute the decay time of phonons. In Chapter 3 the perturbative approach to phonon energies and lifetimes is developed in a Density Functional framework, and the general formula necessary to compute the third order correction is derived and tested. In Chapter 4 the formalism of Chapter 3 is specialized to compute the anharmonic decay of phonons, and the calculated phonon lifetimes in C, Si and Ge are presented along with their pressure and temperature dependence. We conclude the thesis with a Chapter on polar semiconductors, that are characterized by specific theoretical difficulties related to the LO-TO splitting, and for which we present a number of preliminary results.

2 Anharmonic decay of phonons in semiconductors

The interest in the anharmonic decay of phonons has produced a large amount of experimental data. Phonon lifetimes can be measured directly, studying the time evolution of a non-equilibrium phonon population, or indirectly from the width of the Raman peaks. In the last few decades, several attempts have been made to compute phonon lifetimes in semiconductors, leading to a broad range of theoretical results often contrasting with each other and with experimental data. We first briefly summarize the experimental techniques used to measure phonon decay times and we introduce the theory of phonon lifetimes. We then conclude this chapter with a brief review of previous attempts to compute the decay time of phonons.

2.1 What is measured in a Raman experiment?

A typical Raman experiment can be schematized as follows: a photon, inelastically scattered by a sample of material, can create (Stoke process) or destroy (anti-Stoke process) a phonon. By measuring the energy of the scattered photon, we can obtain, from the energy conservation, the frequency of the phonon; if we use visible light as a probe, the momentum of the photon is very small with respect to the reciprocal lattice vectors of typical semiconductors: as a consequence of momentum conservation, we can only observe the creation (or destruction) of phonons very close to the center of the Brillouin zone (the Γ point). In Fig 2.1 we display the typical Raman spectrum of a simple semiconductor. The sharp peak corresponds to one-phonon processes at Γ, the other small features in

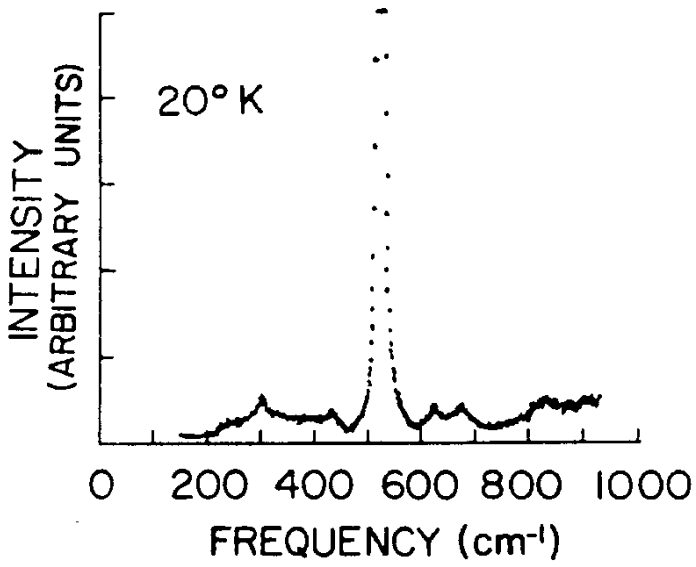

Figure 2.1: The Raman spectrum of Si, from Ref. [4].

the background being due to multi-phonon processes. The one-phonon peak is not perfectly sharp due to the finite lifetime of the phonon. Experimentally it is found that the broadening increases as the temperature is raised (see Fig. 2.2). It is useful to introduce the quantity 2Γ defined as the Full Width at Half Maximum (FWHM) of the one-phonon Raman peak, which is the inverse of the phonon lifetime τ. If we assume that the crystal is free of defects and impurities two different physical effects contribute to the FWHM. The first is isotopic disorder, the second is the anharmonic phonon-phonon interaction. Most elements are found in nature as mixtures of stable isotopes. As an example, we list in Tab. 2.1 the natural abundance of the stable isotopes of carbon, silicon and germanium. The increase of the broadening in the Raman peak due to the presence of different isotopes was studied by Fuchs *et al* [6]. They found that, for natural germanium, the isotopic contribution to the FWHM is very small ($0.017\ \mathrm{cm}^{-1}$) compared to the experimental value of $2\Gamma = 0.89 \pm 0.02\ \mathrm{cm}^{-1}$: this suggest that the most relevant contribution to the broadening

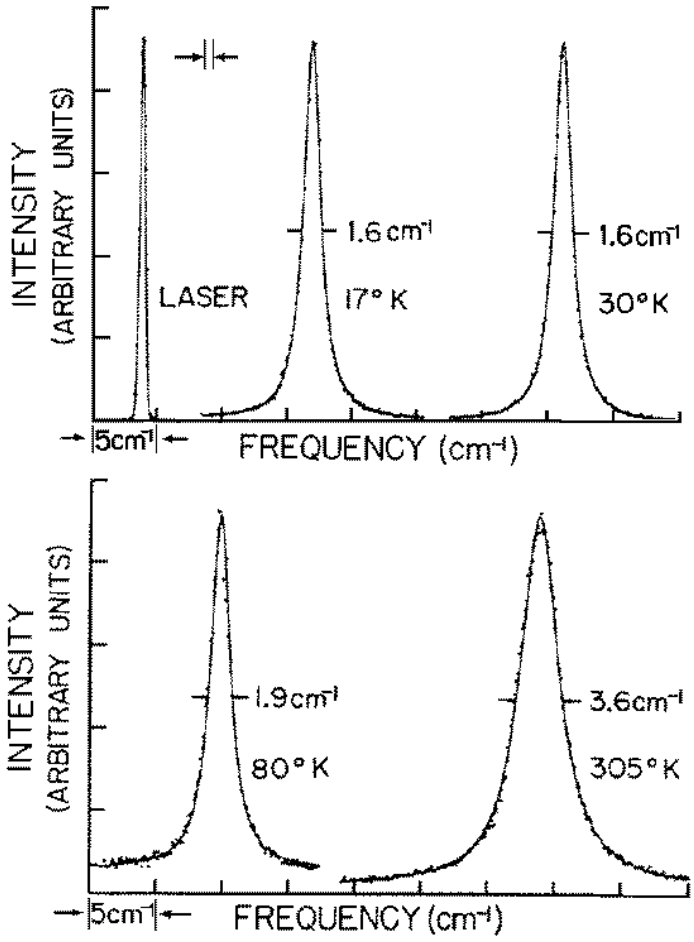

Figure 2.2: The one-phonon Raman line in silicon measured at several temperatures from Ref. [4]. The half-width is indicated on each spectrum.

Table 2.1: Relative abundance of different isotopes of carbon (diamond), silicon and germanium, from Ref. [5].

Diamond	^{12}C 99%	^{13}C 1%			
Silicon	^{28}Si 92%	^{29}Si 5%	^{30}Si 3%		
Germanium	^{70}Ge 21%	^{72}Ge 28%	^{73}Ge 8%	^{74}Ge 37%	^{76}Ge 7%

of the Raman line is due to anharmonic effects.

2.2 Phonon lifetimes from time-resolved experiments

The phonon lifetime can be measured directly using different techniques. One of the most used is the generation of short duration (subnanosecond) coherent phonon packets, through coherent excitation, and the detection of the packet by coherent antistokes Raman scattering (CARS). A full description of this technique can be found in Ref. [7]. A non equilibrium phonon population is generated by two lasers tuned to be in resonance with the zone center phonon frequency. If the durations of the exciting laser pulses are short compared to the relaxation time of the phonon modes, a non-equilibrium phonon population can be generated. These phonons have decay probability per unit of time given by $1/\tau$. This decay process can be monitored by Raman interaction between the vibrational mode and a time delayed third pulsed laser beam. In Fig. 2.3 we report the experimental data obtained by Bron *et al.* for GaP. A similar technique was developed by von der Linde *et al.* [9] in 1980. The main difference with the CARS is that they measure the time evolution of non-equilibrium *incoherent* optical phonons. They observe the generation of optical phonons during the interaction of photoexcited hot electrons and holes with the lattice, and they obtain the relaxation time of a nonequilibrium population of longitudinal optical phonons. Measuring the Raman linewidth is equivalent to measure the time evolution of a non-equilibrium phonon population. The two different experimental methods are complementary as concerns the accuracy of the measurement. Although Raman spectroscopy allows a very accurate measurement of the Raman linewidth, the experimental data are

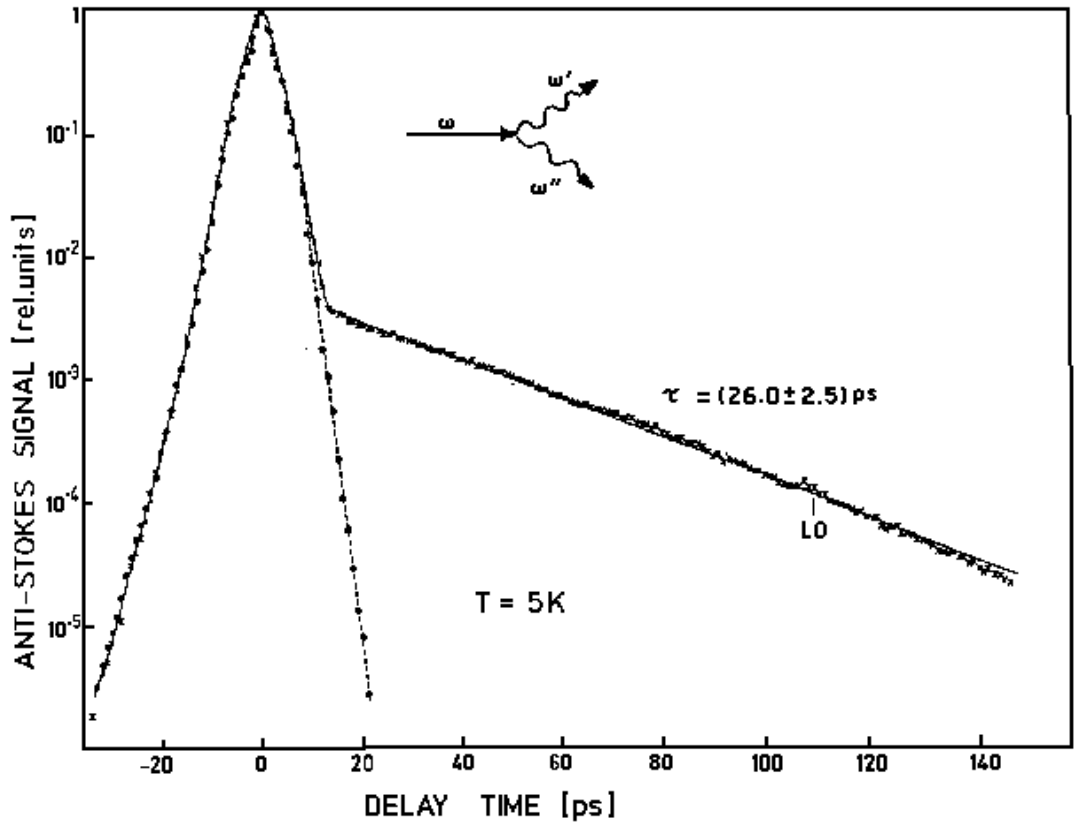

Figure 2.3: Time dependence of CARS signal for GaP at 5K. The component of the signal from ~ -40 to $\sim +20$ ps is primarily due to pump and probe laser beams. In the inset straight line refer to nonequilibrium phonon and wiggly lines refer to thermal phonons. From Ref. [8].

not so reliable when the lifetime is very long, because the corresponding linewidth is to small compared with the width of the laser source. On the contrary, we cannot measure a short lifetime with a time-resolved experiment because the signal is smeared by the laser pulse. An example of comparison between the two techniques can be found in the work by Fuchs *et al.* [6], where they studied the decay time in Germanium. Using time-resolved incoherent picosecond anti-Stoke Raman spectroscopy, they found a phonon lifetime of 8 ± 1 ps in natural Germanium. They also measured the Raman width, obtaining a decay time of 6.0 ± 0.2 ps. According to Fuchs *et al.* "the discrepancy between the *phonon* decay time (determined from the frequency-domain measurements) and the nonequilibrium *phonon population* decay time (determined from time-domain measurements) is due to effects related to the phonon-generation process in the transient experiment".

2.3 Theory of phonon lifetimes

In the following we summarize the procedure which has to be implemented to compute the phonon lifetime. The detailed theory of anharmonic broadening of Raman lines can be found in several review articles (see for example Refs. [10, 2] and references therein).

We indicate the ionic positions at equilibrium as:

$$\mathbf{R}_s^l = \mathbf{R}^l + \tau_s,$$

where l is a cell index and s ($s = 1, ..., n$) is a basis index in the unit cell of n atoms. We introduce the displacements $\{\mathbf{u}_s^l\}$ of the ions from their equilibrium positions; greek subscripts will be used to indicate cartesian components.

The Taylor expansion of the total energy around the equilibrium positions in terms of the displacements reads:

$$E_{tot}(\{\mathbf{u}_s^l\}) = E_{tot}^{(0)} + \frac{1}{2} \sum_{ll',ss',\alpha\beta} \frac{\partial^2 E_{tot}}{\partial u_{s,\alpha}^l \partial u_{s',\beta}^{l'}} u_{s,\alpha}^l u_{s',\beta}^{l'} + \frac{1}{6} \sum_{ll'l'',ss's'',\alpha\beta\gamma} \frac{\partial^3 E_{tot}}{\partial u_{s,\alpha}^l \partial u_{s',\beta}^{l'} \partial u_{s'',\gamma}^{l''}} u_{s,\alpha}^l u_{s',\beta}^{l'} u_{s'',\gamma}^{l''} + \cdots. \quad (2.1)$$

The displacements of the atoms from equilibrium are related to the phonon creation and

annihilation operators, $a_j^+(\mathbf{q})$ and $a_j(\mathbf{q})$, through the usual second quantization formula:

$$u_{s,\alpha}^l = \sum_{\mathbf{q},j} \left(\frac{\hbar}{2\omega_j(\mathbf{q}) M_s N} \right)^{\frac{1}{2}} e_{s,\alpha}(\mathbf{q},j) e^{i\mathbf{q}\cdot\mathbf{R}^l} \left(a_j^+(-\mathbf{q}) + a_j(\mathbf{q}) \right), \tag{2.2}$$

where M_s is the mass of the s-th atom in the unit cell, N is the number of unit cells in the crystal, ω's are the phonon frequencies, the j's indicate the phonon branches ($j = 1 \div 6$ in bulk elemental semiconductors), and $e(\mathbf{q},j)$ is the amplitude of the j-th phonon mode at wavevector $\mathbf{q}$ in the first Brillouin Zone (BZ). Inserting Eq. 2.2 into Eq. 2.1 and retaining only terms up to third order, we obtain that the Hamiltonian of the system is:

$$H = E_{TOT}^{(0)} + H^{harm} + H^{an}, \tag{2.3}$$

where

$$H^{harm} = \sum_{\mathbf{q},j} \hbar\omega_j(\mathbf{q}) \left(a_j^+(\mathbf{q}) a_j(\mathbf{q}) + \frac{1}{2} \right) \tag{2.4}$$

is the harmonic Hamiltonian written is second quantization, and the third order contribution to the Hamiltonian can be written as:

$$H^{an} = \frac{1}{6} \sum_{\mathbf{q},\mathbf{q}',\mathbf{q}''} \sum_{j_1,j_2,j_3} V \begin{pmatrix} \mathbf{q}, & \mathbf{q}', & \mathbf{q}'' \\ j_1, & j_2, & j_3 \end{pmatrix} \left(a_{j_1}^+(-\mathbf{q}) + a_{j_1}(\mathbf{q}) \right) \times \left(a_{j_2}^+(-\mathbf{q}') + a_{j_2}(\mathbf{q}') \right) \left(a_{j_3}^+(-\mathbf{q}'') + a_{j_3}(\mathbf{q}'') \right), \tag{2.5}$$

The coefficients V are related to the third order derivative of the total energy: later on we will display the explicit formula of V for the case we are interested in. The translational invariance of the system gives the conservation law of crystal momentum:

$$\mathbf{q} + \mathbf{q}' + \mathbf{q}'' = \mathbf{G}, \tag{2.6}$$

where $\mathbf{G}$ is a reciprocal lattice vector.

As we can see from Eq. 2.4, the harmonic Hamiltonian does not induce transitions between states with different phonon populations. To study phonon decay times, we consider H^{an} as a perturbation and use the Fermi's golden rule. We thus obtain:

$$\Gamma = \frac{2\pi}{\hbar} \sum_f |\langle i|H^{an}|f\rangle|^2 \, \delta(E_i - E_f), \tag{2.7}$$

where $|i\rangle$ and $|f\rangle$ label the initial and final states respectively, E_i and E_f the corresponding energies, and the delta function ensures the energy conservation.

At thermal equilibrium the phonon population is described by the Bose-Einstein distribution:

$$n_j(\mathbf{q}) = \frac{1}{e^{\hbar\omega_j(\mathbf{q})/kT} - 1}.$$

It is easy to verify that the third order interaction produce no change in such a population, *i.e.* a thermal phonon population is stable, as it was obvious *a priori*. We assume that at $\mathbf{q} = 0$ there is a non-equilibrium phonon population, while in all the other q-points of the Brillouin zone the phonon population is given by the thermal occupation numbers. This is the so called single-mode relaxation time approximation. In our case, only the term in Eq. 2.5 proportional to $a_{LTO}(0)a^+_{j_1}(-\mathbf{q})a^+_{j_2}(\mathbf{q})$ gives a nonvanishing contribution (LTO labels the longitudinal-transverse optical modes). The LTO-phonon at Γ can decay in the same branch (Klemens process, depicted in red in Fig. 2.4), or into two different branches: transverse acoustic (TA) and longitudinal acoustic (LA) branches, transverse acoustic (TA) and transverse optic (TO), and so on. Some of such decay process are sketched in Fig. 2.4. If only three-phonon processes are considered, energy and momentum conservation dictates that the zone-center LTO phonon decays into a pair of phonons with opposite momenta, $\pm\mathbf{q}$, whose frequencies sum up to the frequency of the decaying mode. The inverse lifetime of the LTO mode at zone center reads:

$$\Gamma = \frac{\pi}{2\hbar^2}\sum_{\mathbf{q},j_1,j_2}\left|V\begin{pmatrix}\mathbf{0}, & \mathbf{q}, & -\mathbf{q}\\ LTO, & j_1, & j_2\end{pmatrix}\right|^2 \times \Big(n_{j_1}(\mathbf{q}) + n_{j_2}(-\mathbf{q}) + 1\Big)\delta\Big(\omega_{LTO}(\mathbf{0}) - \omega_{j_1}(\mathbf{q}) - \omega_{j_2}(-\mathbf{q})\Big). \quad (2.8)$$

The matrix elements which determine the width Γ are given by:

$$V\begin{pmatrix}\mathbf{0}, & \mathbf{q}, & -\mathbf{q}\\ LTO, & j_1, & j_2\end{pmatrix} = \sum_{ss's'',\alpha\beta\gamma}\left(\frac{\hbar^3}{8NM_sM_{s'}M_{s''}\omega_{LTO}(\mathbf{0})\omega_{j_1}(\mathbf{q})\partial u_{j_2}(-\mathbf{q})}\right)^{\frac{1}{2}} \times \left(\sum_{l',l''}\frac{\partial^3 E_{tot}}{\partial u^l_{s,\alpha}\partial u^{l'}_{s',\beta}\partial u^{l''}_{s'',\gamma}}e^{i\mathbf{q}\cdot(\mathbf{R}^{l'}-\mathbf{R}^{l''})}\right) e_{s,\alpha}(\mathbf{0},LTO)e_{s',\beta}(\mathbf{q},j_1)e_{s'',\gamma}(-\mathbf{q},j_2) \quad (2.9)$$

The ingredients of the above formula are the harmonic frequencies and displacements, and the third order derivative of the total energy. The former can be computed using standard

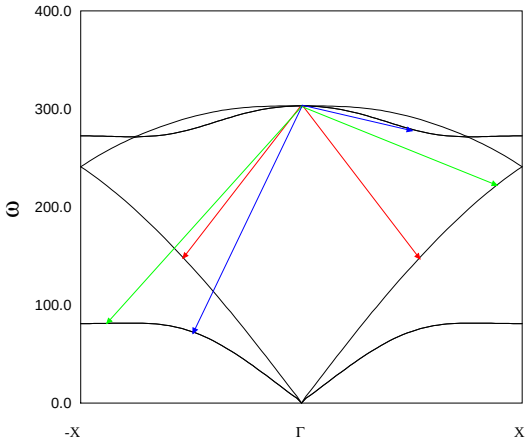

Figure 2.4: (color). Schematic pictures of the decay of LTO-phonon into: TA+LA (green line), LA+LA (red line), TA+TO (blue line).

perturbation theory (see Section 3.3 and Appendix A for theoretical computation, and Appendix G for numerical results); an efficient method to compute the latter is developed in the next chapter.

2.4 Previous attempts to compute phonon lifetimes

The linewidths of optical phonons in simple semiconductors were computed long ago by Klemens [11], Cowley [10], and recently by Narasimhan and Vanderbilt [12]. Their results are reported in Tab. 2.2 and compared with some experimental data. Klemens proposed an analytical model in which the optical phonon can decay only in two acoustic phonons in the same branch. The neglect of the other decay channels resulted in a severe underestimation of linewidths as compared to experiments. Cowley also considered the decay into two different branches obtaining very large values for Si and Ge. Recently Narasimhan and Vanderbilt computed the phonon lifetime in Si using a mixed semi-empirical and ab initio approach. In this work the cubic coupling constants were obtained from an anharmonic Keating-type lattice-dynamical model, which was fitted to a few *ab initio* frozen-phonon calculations. In Ref. [2], Menéndez and Cardona have provided a comprehensive discussion of the limitations of previous theoretical work, pointing out the critical ingredients that need to be taken into account for reliable predictions.

The state of art concerning polar semiconductor is even worse. The most recent theoretical work is due to Usher and Srivastava [14]. They consider the anharmonic term of the lattice Hamiltonian, while treating the crystal as an elastic continuum. The process studied is the decay of a longitudinal optical phonon into acoustic ones. As they pointed out "strictly speaking a continuum crystal cannot support the idea of optic-phonon modes. However $\cdots$ the only way to proceed with the problem at hand is to make this assumption". Using the continuum approximation, the anharmonic part of the crystal Hamiltonian was written in terms of a mode-independent Grüneisen parameter γ, and the phonon lifetime was computed for a wide range of values of Grüneisen constants. The results show that in order to obtain a satisfactory agreement with experimental data one must choose too large a value for Grüneisen constant. For a quantitative comparison, let us consider GaAs: at 77 K the experimental lifetime of LO-phonon is $\tau = 7 \pm 1$ ps (from Ref. [9]), to obtain

Table 2.2: Some experimental and theoretical determinations of the FWHM of Raman phonons at zero temperature. The values corresponding to Klemens's theoretical model are from Ref. [2]. Values given for Cowley model correspond to calculations for 10 K. The data obtained by time resolved experiment are denoted by an asterisk.

Material		FWHM (cm^{-1})
Diamond	Borer[1] *et al.* (expt.)	1.68 ± 0.05
	Klemens[2] (theory)	0.035
	Cowley[3] (theory)	2.74
Silicon	Temple[4] *et al.* (expt.)	1.45 ± 0.05
	Menéndez[5] *et al.* (expt.)	1.24 ± 0.07
	Klemens[2] (theory)	0.048
	Cowley[3] (theory)	11.34
	Narasimhan[6] *et al.* (theory)	0.48
Germanium	Menéndez[5] *et al.* (expt.)	0.75 ± 0.03
	Fuchs[7] *et al.* (expt.)	0.89 ± 0.02
		0.66 ± 0.08*
	Klemens[2] (theory)	0.029
	Cowley[3] (theory)	5.34

[1] Ref. [13, d] [2] Ref. [11]
[3] Ref. [10] [4] Ref. [4]
[5] Ref. [2] [6] Ref. [12]
[7] Ref. [6]

the same value (7 ps) Usher *et al.* must use as input $\gamma = 2.0$, which is four times the experimental value $\gamma \cong 0.5$ suggested by Ref. [15].

3 Perturbation theory in the density-functional framework

In physics only few simple problems can be solved exactly, the solutions of the others requiring the use of some approximations, many of which are based on perturbation theory. The Hamiltonian, in general, can depend on a set of parameters: if we are able to solve our problem for certain values of the parameters (we call the corresponding Hamiltonian "unperturbed"), the solution for values sufficiently "close" to the reference ones can be obtained by a series expansion with respect to the differential parameters.

The use of perturbation theory in the density functional framework was made possible by the work of Baroni, Giannozzi and Testa [16]. In this work they provide an efficient scheme to compute the first order correction to the wavefunction and the second order to the energy. As it was later shown by Gonze and Vigneron [17] and demonstrated below, the first-order correction to the wavefunction is the only quantity we need to compute the correction to the energy of the system up to third order. With this method one was able to compute *ab initio* the full phonon dispersion of semiconductors [18]. Starting from this work many other physical quantities where investigated from first principles; among them we quote the elastic constants [19], dielectric and piezoelectric constants [20], and various other lattice-dynamical properties [21, 22].

All the applications of density functional perturbation theory (DFPT) appeared so far are limited to second order in the energy. It is a well known result of elementary quantum-mechanics that the knowledge of the wavefunction response of a system up to n-th order in the strength of an external perturbation is sufficient to determine the energy derivative up

to order $2n+1$ [23]. The validity of this '$2n+1$ theorem' within self-consistent field (SCF) theories has been known since several years in the quantum-chemistry community [24], and recently it has been generalized to density-functional theory (DFT) by Gonze and Vigneron [17]. A first important conclusion we can draw from this 'theorem' is that the knowledge of the *linear* response of a system to an external perturbation allows one to determine the *third* derivatives of the energy with respect to the strength of the perturbation and it gives therefore a practical way to link linear and quadratic generalized susceptibilities. The interest in doing so is evident: one can in principle obtain higher-order susceptibilities or gain in the accuracy achieved by perturbation theory essentially *for free*.

In the first section of this chapter we review some applications of perturbation theory. In Section 3.2 we introduce the DFT formalism. Following the formulation of Gonze and Vigneron we will state in Section 3.3 the "$2n+1$" theorem in the case n=1. We then restate the Gonze and Vigneron formula in a form which is free from some of its original drawbacks, and is well suited for practical implementations. As an example, we calculate the third-order anharmonic coupling coefficients in Silicon at some high-symmetry points of the Brillouin zone, and compare them with results obtained by the frozen-phonon method.

3.1 Why is it useful ?

There are many physical quantities that can be measured by applying a small perturbation to the material. For example, we may consider the displacements of the atoms from the equilibrium positions as perturbation parameters; phonon frequencies can be obtained from the second derivatives of the crystal's energy, while third derivatives determine the phonon lifetimes, which are the subject of the present thesis. Linear response functions are an important example of physical quantities which are second derivatives of the energy. In order to illustrate this, let us consider the response of a system to an external uniform electric field $\vec{\mathcal{E}}$. The variable conjugate to $\vec{\mathcal{E}}$ in the energy expansion is the displacement field

$$\vec{\mathcal{D}} = -\frac{4\pi}{V}\frac{\partial E}{\partial \mathcal{E}}$$

where V is the crystal volume. The displacement field is also given by $\vec{\mathcal{D}} = \epsilon\vec{\mathcal{E}}$ where ϵ is the dielectric tensor. Combining the two relations we can easily see that the dielectric tensor is proportional to the second derivative of the energy with respect an electric field. As a second example, let us consider elasticity. The second derivatives of the energy with respect to strain are the elastic constants. The solid can also interact at the same time with two perturbations of different kind: in this case we must consider mixed derivatives. For example, the piezoelectric tensor is the second derivative of the energy with respect to electric field and strain. A third order derivative with respect to twice an electric field and a phonon displacement gives the Raman tensor. By definition, the various response functions describe the behavior of the system in the limit where the strength of the perturbation becomes infinitely small.

On the other hand, perturbation theory also allows to calculate properties of specific, complex, materials which can viewed as small perturbations with respect to some other, simpler, system. In these cases the magnitude of the perturbation is fixed. The applications belonging to this second group are based on the so called *computational alchemy* approach to semiconductor alloys [25] and superlattices [26], in which the disordered semiconductor is viewed as a small perturbation with respect to a reference, periodic system composed of fictitious *virtual* atoms. By ideally applying a perturbation which restore for every atom the potential of the corresponding atomic species, one obtains the physical material one wants to study. In this way, properties of very large supercells can be computed by solving the Hamiltonian for the virtual crystal, which requires a small cell, and then applying perturbation theory.

3.2 Density functional theory

In 1964 Hohenberg and Kohn [27] demonstrated that all the properties of the nondegenerate ground state of a system of interacting electrons are completely determined by its electron density $n(\mathbf{r})$. From this work density functional theory has evolved as a conceptually and practically useful method for studying the electronic properties of many-electron systems. These properties can be calculated from first principles, *i.e.* DFT calculations do not need any experimental input or adjustable parameters to accurately predict many

physical quantities. Structural properties have been obtained using the so called local density approximation, resulting in typical errors with respect to the experimental data of a few percents only (for a review see Ref. [28]).

In the Kohn-Sham [29] (KS) formulation of DFT, the total energy of an electronic system in an external field $v_{\rm ext}$, is given by:

$$E[n] = \sum_\alpha \epsilon_\alpha - \frac{1}{2} \int \frac{n(\mathbf{r})\, n(\mathbf{r}')}{|\mathbf{r} - \mathbf{r}'|}\, \mathrm{d}\mathbf{r}\, \mathrm{d}\mathbf{r}' + E_{\rm xc}[n] - \int \frac{\delta E_{\rm xc}[n]}{\delta n(\mathbf{r})}\, n(\mathbf{r})\, \mathrm{d}\mathbf{r},$$

where $\frac{\delta E_{\rm xc}[n]}{\delta n(\mathbf{r})}$ indicates the functional derivative of the exchange and correlation energy, the ϵ_α are the eigenvalues of the Kohn-Sham one-particle equations:

$$H|\psi_\alpha\rangle = \epsilon_\alpha\, |\psi_\alpha\rangle, \qquad \langle\psi_\alpha|\psi_\alpha\rangle = 1; \tag{3.1}$$

with the self-consistent Hamiltonian H given by :

$$H = -\frac{1}{2}\nabla^2 + v_{\rm ext} + \frac{\delta E_I[n]}{\delta n(\mathbf{r})}, \tag{3.2}$$

where we have defined the "interaction energy" $E_I[n]$ as:

$$E_I[n] = \frac{1}{2} \int \frac{n(\mathbf{r})\, n(\mathbf{r}')}{|\mathbf{r} - \mathbf{r}'|}\, \mathrm{d}\mathbf{r}\, \mathrm{d}\mathbf{r}' + E_{\rm xc}[n]. \tag{3.3}$$

The ground state density of the system is:

$$n(\mathbf{r}) = \sum_\alpha \psi^*_\alpha(\mathbf{r})\, \psi_\alpha(\mathbf{r}), \tag{3.4}$$

where the sum runs over occupied (*valence*) Kohn-Sham orbitals.

The KS equations must be solved self-consistently. Starting from a trial density Eq. 3.1 is solved; using the eigenfunctions so obtained and Eq. 3.4 the new density is then computed; with the new density one solves again Eq. 3.1 and one iterates the cycle until self-consistences is achieved. In this way the ground state density can be computed along with the corresponding energy.

3.2.1 The local density approximation

To implement Eq. 3.2 we need an explicit expression for the exchange and correlation energy functional; for a system with slowly varying density we can use the so called Local Density Approximation (LDA):

$$E_{xc}[n] = \int \epsilon_{xc}(n(\mathbf{r}))n(\mathbf{r})d\mathbf{r}, \tag{3.5}$$

where $\epsilon_{xc}(n)$ is the exchange and correlation energy per particle of a uniform electron gas of density n. In spite of its simplicity LDA has given very good results well beyond its strict applicability range, *e.g.* for the rather inhomogeneous tetrahedrally bonded semiconductors.

3.3 Density functional perturbation theory

When the *external* potential depends on a parameter, λ we can perform a Taylor expansion:

$$v_{ext}(\mathbf{r},\lambda) \equiv v_{ext}^{(0)}(\mathbf{r}) + \lambda v_{ext}^{(1)}(\mathbf{r}) + \lambda^2 v_{ext}^{(2)}(\mathbf{r}) + \cdots. \tag{3.6}$$

Also the KS wave functions may be expanded in the same way:

$$\psi(\lambda) = \psi^{(0)} + \lambda\psi^{(1)} + \lambda^2\psi^{(2)} + \lambda^3\psi^{(3)} + \cdots, \tag{3.7}$$

along with the corresponding power series for the energy,

$$E[n,\lambda] = E^{(0)}[n] + \lambda E^{(1)}[n] + \lambda^2 E^{(2)}[n] + \lambda^3 E^{(3)}[n] + \cdots. \tag{3.8}$$

A remarkable help in the computation of the correction in the energy expansion is provided by the so called "$2n+1$" theorem. This theorem states that the knowledge of all the corrections to the wavefunction up to $\psi^{(n)}$ is sufficient to determine all the correction to the energy up to $E^{(2n+1)}$ (see, for example, Ref. [30]). In this thesis we are interested in third-order corrections to the energy, thus we have to compute only the first order correction to the wavefunction.

3.3.1 Second order and linear response

The second order correction to the energy can be easily computed from the Hellmann-Feynman theorem which states that the generalized force associated with a variation of the external parameter λ is given by the ground-state expectation value of the derivative of $v_{ext}(\mathbf{r},\lambda)$:

$$\frac{\partial E[n,\lambda]}{\partial \lambda} = \int n(\mathbf{r},\lambda)\frac{\partial v_{ext}(\mathbf{r},\lambda)}{\partial \lambda} d\mathbf{r}, \tag{3.9}$$

where $n(\mathbf{r},\lambda)$ is the electronic ground-state density corresponding to a given value of λ. Deriving the above equation with respect to λ and substituting the corresponding terms in the Taylor expansions 3.6 and 3.8, one obtains:

$$E^{(2)}[n] = \int \left(\frac{1}{2}n^{(1)}(\mathbf{r})v^{(1)}_{ext}(\mathbf{r}) + n^{(0)}(\mathbf{r})v^{(2)}_{ext}(\mathbf{r})\right) d\mathbf{r}, \tag{3.10}$$

where $n^{(0)}$ is the unperturbed electronic ground-state density and $n^{(1)}(\mathbf{r})$ is the first derivative with respect to λ.

To evaluate the second order correction to the total energy one must solve the first order problem, *i.e.* obtain the linear response of the system to an external perturbation. One has to compute self-consistently the first order correction to the Hamiltonian:

$$H^{(1)} = v^{(1)}_{\mathrm{ext}} + \int \frac{\delta^2 E_I[n]}{\delta n(\mathbf{r})\, n(\mathbf{r}')}\, n^{(1)}(\mathbf{r}')\, \mathrm{d}\mathbf{r}' \tag{3.11}$$

The linearization in the parameter λ of the KS equations, 3.1, gives

$$\left(H^{(0)} - \epsilon^{(0)}_\alpha\right)\left|\psi^{(1)}_\alpha\right\rangle = -\left(H^{(1)} - \epsilon^{(1)}_\alpha\right)\left|\psi^{(0)}_\alpha\right\rangle, \tag{3.12}$$

where the first order correction to the KS-eigenvalue is:

$$\epsilon^{(1)}_\alpha = \left\langle \psi^{(0)}_\alpha \middle| H^{(1)} \middle| \psi^{(0)}_\alpha \right\rangle. \tag{3.13}$$

Eq. 3.12 and Eq. 3.13 are the standard first-order equations of perturbation theory. The orthogonality condition to the first order wavefunction

$$\mathrm{Re}\left\langle \psi^{(0)}_\alpha \middle|\, \psi^{(1)}_\alpha \right\rangle = 0 \tag{3.14}$$

must be imposed. From $\psi^{(1)}$ one computes the first order density as:

$$n^{(1)}(\mathbf{r}) = \sum_{\alpha} \left[\psi_{\alpha}^{(1)^*}(\mathbf{r})\, \psi_{\alpha}^{(0)}(\mathbf{r}) + \psi_{\alpha}^{(0)^*}(\mathbf{r})\, \psi_{\alpha}^{(1)}(\mathbf{r}) \right] . \tag{3.15}$$

The above set of equations must be solved self-consistently. The first iteration usually starts with $H^{(1)} = v_{\text{ext}}^{(1)}$, and Eq. (3.12) is subsequently solved for all the first-order corrections of valence states α, with the constraints expressed by Eq. (3.14). The first-order charge density is then computed by Eq. (3.15); this allows one to calculate a relaxed first-order Hamiltonian as in Eq. (3.11). The Hamiltonian is then inserted in Eqs. (3.13) and (3.12), and the process is iterated until self-consistency is achieved. In the special case of a degenerate unperturbed eigenvalue, one must use standard perturbation theory choosing the unperturbed (degenerate) wavefunctions so as to satisfy the relation:

$$\epsilon_{\alpha}^{(1)}\, \delta_{\alpha\beta} = \left\langle \psi_{\alpha}^{(0)} \middle| H^{(1)} \middle| \psi_{\beta}^{(0)} \right\rangle \tag{3.16}$$

3.4 Higher orders

Applying the $2n + 1$ theorem to the case $n = 1$ one is able to write the third order correction to the energy using only the first order correction to the valence wavefunction. The third order expression depends not only on $n^{(1)}$, but also on $\psi^{(1)}$. The demonstration of the $2n + 1$ theorem in the density functional framework was provided by Gonze and Vigneron [17], who also gave a general formula valid at all orders. Their demonstration for the case $n = 1$ is reported in Appendix B; here we just state their result. According to Gonze and Vigneron the third-order derivative of the DFT ground-state energy with respect to λ reads:

$$\begin{aligned} E^{(3)} &= \sum_{\alpha} \left[\left\langle \psi_{\alpha}^{(1)} \middle| \, H^{(1)} - \epsilon_{\alpha}^{(1)} \, \middle| \psi_{\alpha}^{(1)} \right\rangle \right] \\ &+ \int v_{\text{ext}}^{(2)}(\mathbf{r}) n^{(1)}(\mathbf{r}) d\mathbf{r} + \int v_{\text{ext}}^{(3)}(\mathbf{r}) n^{(0)}(\mathbf{r}) d\mathbf{r} \\ &+ \frac{1}{6} \int \frac{\delta^3 E_{xc}[n]}{\delta n(\mathbf{r}) \delta n(\mathbf{r}') \delta n(\mathbf{r}'')}\, n^{(1)}(\mathbf{r})\, n^{(1)}(\mathbf{r}')\, n^{(1)}(\mathbf{r}'')\, \mathrm{d}\mathbf{r}\, \mathrm{d}\mathbf{r}'\, \mathrm{d}\mathbf{r}''. \end{aligned} \tag{3.17}$$

Eq. 3.17 clearly shows that the calculation of the third-order correction to the energy requires only the knowledge of such ingredients as $\psi^{(1)}$ and $\epsilon^{(1)}$ which are directly accessible to first-order perturbation theory.

3.4.1 A new formula

All the results of DFT must be invariant with respect to unitary transformations of the orbitals which do not mix the manifolds of occupied (*valence*) and empty (*conduction*) states. As it stands, Eq. 3.17 does not manifestly display this invariance. Furthermore, its implementation would require the knowledge of the components of the perturbed wavefunction,[1] ψ_v^1, over all the valence wavefunctions different from ψ_v^0 itself: $\langle\psi_{v'}^0|\psi_v^1\rangle_{v'\neq v}$. Again, this is not natural because in DFT the variation of any physical property must only depend on the variation of the one-electron density matrix which is not affected by components of the perturbed valence orbital along the unperturbed valence manifold. This situation is particularly unpleasant when, due to the degeneracy or quasi-degeneracy of some unperturbed valence states, the actual implementation of Eq. 3.17 would require the use of degenerate-state perturbation theory. When λ goes to zero the perturbed wavefunction approaches the unperturbed one. If the unperturbed eigenstate is degenerate the choice of the corresponding wave function is not unique; the right choice is a linear combination of unperturbed (degenerate) eigenvectors that satisfy Eq. 3.16.

We will now show that Eq. 3.17 can be recast in a form which requires only the knowledge of the conduction-manifold projection of the ψ_v^1's, which is manifestly invariant with respect to unitary transformations within the valence manifold, and which can be straightforwardly and efficiently implemented using standard non-degenerate first-order perturbation theory [31].

The second, third and fourth terms on the rhs of Eq. 3.17 already display the desired unitary invariance. We concentrate on the first term of Eq. 3.17. Our final result is:

$$\sum_v \langle\psi_v^1|H^1 - \epsilon_v^1|\psi_v^1\rangle = \sum_v \langle\psi_v^1|P_c H^1 P_c|\psi_v^1\rangle - \sum_{vv'} \langle\psi_v^1|P_c|\psi_{v'}^1\rangle\langle\psi_{v'}^0|H^1|\psi_v^0\rangle, \qquad (3.18)$$

[1] To simplify the notation, in the rest of this section we suppress the parenthesis in the apex; so *e.g.* ψ^1 indicates the first order correction to the wavefunction, the same is done for the other quantities.

where $P_c \equiv \sum_c |\psi_c^0\rangle\langle\psi_c^0|$ is the projector over the unperturbed conduction-state manifold (from now on, 'c' will indicate an index running over conduction states, while 'v' indicates valence states). Before demonstrating Eq. 3.18 we notice that it is manifestly invariant with respect to unitary transformations within the valence manifold. In fact, it is the sum of the trace of a matrix defined over that manifold (first term on the rhs) and of the product of two such matrices (second term). The desired invariance derives from the invariance property of the trace.

The demonstration of Eq. 3.18 is tedious, but straightforward. Let us start from the definition of the first-order correction to the v-th unperturbed valence state, and consider its projections over the valence- and conduction-state manifolds:

$$|\psi_v^1\rangle = P_c|\psi_v^1\rangle + P_v|\psi_v^1\rangle, \tag{3.19}$$

$$P_c|\psi_v^1\rangle = \sum_c |\psi_c^0\rangle \frac{\langle\psi_c^0|H^1|\psi_v^0\rangle}{\epsilon_v^0 - \epsilon_c^0}, \tag{3.20}$$

$$P_v|\psi_v^1\rangle = \sum_{v'\neq v} |\psi_{v'}^0\rangle \frac{\langle\psi_{v'}^0|H^1|\psi_v^0\rangle}{\epsilon_v^0 - \epsilon_{v'}^0}, \tag{3.21}$$

where $P_v \equiv 1 - P_c$ is the projector over the valence manifold.

Substituting Eq. (3.19) into the left-hand size of Eq. 3.18, one obtains the sum of four terms, which will be denoted by cc, cv, vc, and vv, according to the couple of projectors appearing inside the matrix elements. Inserting Eq. (3.21) into the expression of the vv term and separating out terms with $v' = v''$ from those with $v' \neq v''$, one obtains:

$$\sum_v \langle\psi_v^1|P_v(H^1 - \epsilon_v^1)P_v|\psi_v^1\rangle = \sum_{v\neq v'} \frac{\langle\psi_v^0|H^1|\psi_{v'}^0\rangle(\epsilon_{v'}^1 - \epsilon_v^1)\langle\psi_{v'}^0|H^1|\psi_v^0\rangle}{(\epsilon_v^0 - \epsilon_{v'}^0)^2} + \\ + \sum_{v\neq v'\neq v''} \frac{\langle\psi_v^0|H^1|\psi_{v'}^0\rangle\langle\psi_{v'}^0|H^1|\psi_{v''}^0\rangle\langle\psi_{v''}^0|H^1|\psi_v^0\rangle}{(\epsilon_v^0 - \epsilon_{v'}^0)(\epsilon_v^0 - \epsilon_{v''}^0)}. \tag{3.22}$$

Both terms on the rhs of Eq. 3.22 vanish because the parities of the numerators and those of the denominators with respect to the exchanges $v \rightleftharpoons v'$ $v \rightleftharpoons v''$ are different. Let us come now to the cv and vc terms. Using Eqs. (3.20) and (3.21) and a few algebraic manipulations, one obtains:

$$\sum_v \Big(\langle\psi_v^1|P_c(H^1 - \epsilon_v^1)P_v|\psi_v^1\rangle + \langle\psi_v^1|P_v(H^1 - \epsilon_v^1)P_c|\psi_v^1\rangle \Big) =$$

$$\sum_{c,v\neq v'} \frac{\langle\psi_v^0|H^1|\psi_c^0\rangle\langle\psi_c^0|H^1|\psi_{v'}^0\rangle\langle\psi_{v'}^0|H^1|\psi_v^0\rangle}{(\epsilon_v^0-\epsilon_{v'}^0)}\left(\frac{1}{\epsilon_v^0-\epsilon_c^0}-\frac{1}{\epsilon_{v'}^0-\epsilon_c^0}\right)= -\sum_{c,v\neq v'}\frac{\langle\psi_v^0|H^1|\psi_c^0\rangle\langle\psi_c^0|H^1|\psi_{v'}^0\rangle\langle\psi_{v'}^0|H^1|\psi_v^0\rangle}{(\epsilon_v^0-\epsilon_c^0)(\epsilon_{v'}^0-\epsilon_c^0)}. \tag{3.23}$$

The *cc* term reads:

$$\sum_v\langle\psi_v^1|P_c(H^1-\epsilon_v^1)P_c|\psi_v^1\rangle = \sum_v\langle\psi_v^1|P_cH^1P_c|\psi_v^1\rangle-\sum_{c,v}\frac{\langle\psi_v^0|H^1|\psi_c^0\rangle\langle\psi_c^0|H^1|\psi_v^0\rangle\langle\psi_v^0|H^1|\psi_v^0\rangle}{(\epsilon_v^0-\epsilon_c^0)(\epsilon_v^0-\epsilon_c^0)}. \tag{3.24}$$

The first term on the rhs of Eq. 3.24 coincides with the first term on the rhs of Eq. 3.18. The second term has the same form as the rhs of Eq. 3.23, just providing the $v=v'$ terms which were missing therein. By combining these terms, we finally obtain:

$$\sum_v\langle\psi_v^1|H^1-\epsilon_v^1|\psi_v^1\rangle = \sum_v\langle\psi_v^1|P_cH^1P_c|\psi_v^1\rangle- -\sum_{c,v}\frac{\langle\psi_v^0|H^1|\psi_c^0\rangle\langle\psi_c^0|H^1|\psi_{v'}^0\rangle\langle\psi_{v'}^0|H^1|\psi_v^0\rangle}{(\epsilon_v^0-\epsilon_c^0)(\epsilon_{v'}^0-\epsilon_c^0)}. \tag{3.25}$$

By using Eq. (3.20) and the condition that different conduction state are orthogonal to each other, we finally arrive at Eq. 3.18.

3.4.2 Dealing with more than one perturbation

Eq. 3.18 can be easily generalized to the case where the perturbation depends on more than one parameter (as it is the case, e.g., in lattice dynamics where the λ's are different nuclear displacements). Suppose there are three such parameters, $\{\lambda_1,\lambda_2,\lambda_3\}$. Following the notation and the line of reasoning of Ref. [17], one define

$$E^{\lambda_1\lambda_2\lambda_3}\equiv\frac{1}{6}\frac{\partial^3E}{\partial\lambda_1\partial\lambda_2\partial\lambda_3}.$$

One can easily convince ourself that:

$$E^{\lambda_1\lambda_2\lambda_3}=\frac{1}{6}\left(\widetilde{E}^{\lambda_1\lambda_2\lambda_3}+\widetilde{E}^{\lambda_2\lambda_1\lambda_3}+\widetilde{E}^{\lambda_1\lambda_3\lambda_2}+\widetilde{E}^{\lambda_3\lambda_1\lambda_2}+\widetilde{E}^{\lambda_3\lambda_2\lambda_1}+\widetilde{E}^{\lambda_2\lambda_3\lambda_1}\right), \tag{3.26}$$

where

$$\widetilde{E}^{\lambda_1\lambda_2\lambda_3} = \sum_v \langle\psi_v^{\lambda_1}|P_c H^{\lambda_2} P_c|\psi_v^{\lambda_3}\rangle - \sum_{vv'}\langle\psi_v^{\lambda_1}|P_c|\psi_{v'}^{\lambda_2}\rangle\langle\psi_{v'}^0|H^{\lambda_3}|\psi_v^0\rangle + \int n^{\lambda_1}(\mathbf{r})v^{\lambda_2\lambda_3}(\mathbf{r})d\mathbf{r} + \int v^{\lambda_1\lambda_2\lambda_3}(\mathbf{r})n^0(\mathbf{r})d\mathbf{r} + \frac{1}{6}\int \frac{\delta^3 E_{xc}[n]}{\delta n(\mathbf{r})\delta n(\mathbf{r}')\delta n(\mathbf{r}'')} n^{\lambda_1}(\mathbf{r})n^{\lambda_2}(\mathbf{r}')n^{\lambda_3}(\mathbf{r}'')d\mathbf{r}d\mathbf{r}'d\mathbf{r}'', \quad (3.27)$$

and the superscripts λ_i indicate derivatives with respect to λ_i. One sees that when the external potential depends linearly on just one parameter, λ, Eq. 3.17 is recovered. These formulas are completely general and can be applied to atoms and molecules as well as to periodic systems; in the latter case the wave-functions have the usual Bloch's form. [2]

In the general case where the positions of the nuclei also depend on the λ's, one must of course add to Eq. 3.26 the derivative of the ionic contribution to the energy which is usually expressed as an Ewald sum. All the ingredients necessary to implement Eq. 3.27 are naturally provided by any computer code aimed at standard second-order DFPT, such as the one we routinely use for lattice-dynamical calculations. In summary, the main advantages of this new formulation are the following: i) Using the projector over the conduction state manifold the expression of the energy is well defined in the case of semiconductors since the denominator appearing in Eq. 3.20 never vanishes; ii) With Eq. 3.27 one do not need any particular choice of the degenerate valence manifold.

3.4.3 A numerical test

To test our formulation, we have compared results obtained from Eq. 3.27 for some lattice distortions in Si, with those obtained by the frozen phonon method: this can only be done for perturbations of very short wave-length, typically a few lattice spacings at most. In the frozen phonon approach, the total energy is calculated self-consistently for a series of lattice distortions. Once the dependence of the total energy on atomic displacements is calculated, one obtains the atomic force constants and phonon frequencies from the second

[2]Different perturbation can be applied to a periodic solids, between them a uniform electric field does not present periodic boundary conditions, in Appendix C we provide a simple recipes to solve this problem.

derivatives of the energy (or the first derivatives of the forces), while the third derivatives are related to the anharmonic couplings.

In the following, we present some tests of the above formulation which we have made on the anharmonic coupling between lattice distortions of Silicon at selected high-symmetry points of the BZ. The details of the frozen phonon calculation are presented in Appendix D. The equilibrium and lattice-dynamical properties of Silicon have been calculated within the local-density approximation, using the plane-wave pseudopotential method. We have used the same pseudopotential as in Ref. [21], plane waves up to a kinetic-energy cutoff of 14 Ry, and the (444) Monkhorst-Pack mesh for BZ integrations [32]. Calculations have been done at the Γ and X points of the BZ. The distorted cells have a lower (rotational and/or translational) symmetry, and the set of $\mathbf{k}$-point used for sampling the BZ has been modified accordingly. We stress that, as it is the case for the harmonic dynamical matrix [21], the calculation of anharmonic coefficients at arbitrary points of the BZ within DFPT does *not* require the use of any supercells, but it only uses wavefunctions and band energies calculated for the unperturbed system. There are four independent parameters describing the harmonic properties of the crystal within the set of distortions corresponding to Γ and X phonons (the Γ_{LTO}, X_{LAO}, X_{TA}, and X_{TO} frequencies), whereas there are six anharmonic constants: one describing the coupling between three Γ-like phonons, and five describing the coupling between one Γ- and two X-like phonons. We refer to Ref. [33] for a full group-theoretical analysis of the independent coupling coefficients, for an explanation of the notations, see Appendix D. In Table 3.1 we compare the third-order coupling coefficients calculated in the present work with DFPT and the frozen-phonon method [31]. The values obtained with the latter method result from a procedure analogous to the one used in Ref. [33]. As one can see, DFPT gives results which are in excellent agreement with those obtained by the frozen-phonon method. Actually, they are in principle more accurate because DFPT directly provides the energy derivatives without the need of any numerical differentiations. We conclude that DFPT provides an accurate and computationally convenient tool for calculating the anharmonic coupling of phonons at arbitrary points of the BZ, with a numerical effort which essentially does not depend on the position in the BZ. This opens the way to a systematic investigation of such effects in real materials.

Table 3.1: Comparison of the third-order anharmonic coupling constants between phonons at the Γ and X points of the Brillouin zone in Silicon, as obtained by density-functional perturbation theory (DFPT) and the frozen-phonon (FP) method. The notations are the same as in Ref. [12]. Units are eV/Å^3 (from Ref. [31]).

	B_{xyz}	$I_{z\overline{aa}}$	$I_{\overline{zbb}}$	$I_{z\overline{cc}}$	$I_{\overline{xac}}$	$I_{\overline{ybc}}$
DFPT	-295.06	232.41	-35.27	55.92	447.64	-64.74
FP	-295.27	232.11	-35.23	55.44	447.19	-64.84

4 Phonon lifetimes in semiconductors

In the previous chapter we have shown how third-order perturbation theory can be implemented using ingredients which are byproducts of standard ab-initio lattice dynamical calculations in the harmonic approximation, thus requiring a similar computational effort and resulting in a similar accuracy. In this chapter we show that anharmonic lifetimes of semiconductors can be determined within a predictive theoretical scheme, allowing a full understanding of the detailed microscopic processes which lead to phonon decay. Our method is demonstrated by calculating the phonon lifetimes in diamond, Si and Ge, along with their temperature and pressure dependences. Our results, which are in good agreement with available experimental data, allow a clear understanding of the relative importance of different decay mechanisms, and open the possibility to study modifications of lifetimes which can be induced through external parameters (such as e.g. pressure and materials engineering) by affecting the relative importance of individual decay channels.

4.1 Analytical formulation

To evaluate the decay time of phonons from Eq. 2.8 we have to compute the third derivative of the total energy of the system (Eq. 3.26) with respect atomic displacements from the equilibrium position $\{\mathbf{u}_s^l\}$. The Taylor expansion of the total energy around the equilibrium positions in terms of the displacements reads:

$$E_{tot}(\{\mathbf{u}_s^l\}) = E_{tot}^{(0)} + E_{tot}^{(2)}(\{\mathbf{u}_s^l\}) + E_{tot}^{(3)}(\{\mathbf{u}_s^l\}) + \cdots. \tag{4.1}$$

The second order term is given by:

$$E^{(2)}_{tot}(\{\mathbf{u}^l_s\}) = \frac{1}{2}\sum_{ll',ss',\alpha\beta} C_{ss',\alpha\beta}(l,l')u^l_{s,\alpha}u^{l'}_{s',\beta}, \tag{4.2}$$

where the harmonic force constants are the second derivatives of the total energy:

$$C_{ss',\alpha\beta}(l,l') = \frac{\partial^2 E_{tot}}{\partial u^l_{s,\alpha}\partial u^{l'}_{s',\beta}}. \tag{4.3}$$

Analogously, the anharmonic force constants are the third derivatives of the energy and may be defined through:

$$E^{(3)}_{tot}(\{\mathbf{u}^l_s\}) = \frac{1}{6}\sum_{ll'l'',ss's'',\alpha\beta\gamma} C_{ss's'',\alpha\beta\gamma}(l,l',l'')u^l_{s,\alpha}u^{l'}_{s',\beta}u^{l''}_{s'',\gamma}, \tag{4.4}$$

where

$$C_{ss's'',\alpha\beta\gamma}(l,l',l'') = \frac{\partial^3 E_{tot}}{\partial u^l_{s,\alpha}\partial u^{l'}_{s',\beta}\partial u^{l''}_{s'',\gamma}}. \tag{4.5}$$

From the harmonic force constants one can obtain the dynamical matrix and compute the phonon frequencies. The procedure is developed in Appendix A. Let us introduce the reciprocal-space anharmonic force constant defined as:

$$C_{ss's'',\alpha\beta\gamma}(\mathbf{q},\mathbf{q}',\mathbf{q}'') = \frac{1}{N}\sum_{l,l',l''} C_{ss's'',\alpha\beta\gamma}(l,l',l'')e^{i\mathbf{q}\cdot\mathbf{R}^l}e^{i\mathbf{q}'\cdot\mathbf{R}^{l'}}e^{i\mathbf{q}''\cdot\mathbf{R}^{l''}}, \tag{4.6}$$

where the $\mathbf{q}$'s are in the first Brillouin zone. We call $C_{ss's'',\alpha\beta\gamma}(\mathbf{q},\mathbf{q}',\mathbf{q}'')$ the third order *dynamical tensor*, in analogy to the second order case. We recall that the translational invariance of the system gives the condition:

$$\mathbf{q}+\mathbf{q}'+\mathbf{q}'' = \mathbf{G}, \tag{4.7}$$

where $\mathbf{G}$ is a reciprocal lattice vector. We can easily recognize that $C_{ss's'',\alpha\beta\gamma}(\mathbf{0},\mathbf{q},-\mathbf{q})$ is the anharmonic term which appears in parenthesis in the last line of Eq. 2.9. The atomic displacement in reciprocal space is defined as:

$$\mathbf{u}_s(\mathbf{q}) = \sum_l \mathbf{u}^l_s e^{i\mathbf{q}\cdot\mathbf{R}^l}$$

In the following, for simplicity, we replace the double index (s,α) with p ($p = 1, \cdots, 3n$). Using the formula for the derivative of composed functions, we rewrite the anharmonic tensor in term of derivative with respect to $\mathbf{u}(\mathbf{q})$:

$$C_{p,p',p''}(\mathbf{q}_1,\mathbf{q}_2,\mathbf{q}_3) = \frac{\partial^3 E_{tot}}{\partial u_p(\mathbf{q})\partial u_{p'}(\mathbf{q}')\partial u_{p''}(\mathbf{q}'')}. \tag{4.8}$$

We specialize now Eqs. 3.26 and 3.27 to our case where the perturbing parameter λ is given by the phonon displacements $u_p(\mathbf{q})$. In our case, $\tilde{E}$, which appears in Eq. 3.27, is the sum of an electronic part $\tilde{E}^{el}$ plus an ionic contribution $\tilde{E}^{ion}$, which is essentially the third derivative of an Ewald sum whose expression is given in Appendix E:

$$\tilde{E}_{pp'p''}(\mathbf{q}_1,\mathbf{q}_2,\mathbf{q}_3) = \tilde{E}^{el}_{pp'p''}(\mathbf{q}_1,\mathbf{q}_2,\mathbf{q}_3) + \tilde{E}^{ion}_{pp'p''}(\mathbf{q}_1,\mathbf{q}_2,\mathbf{q}_3).$$

With the help of Eq. 3.27, we find for the electronic contribution:

$$\begin{aligned}
&\tilde{E}^{el}_{pp'p''}(\mathbf{q}_1,\mathbf{q}_2,\mathbf{q}_3) = \\
&\sum_v \Big\langle \frac{\partial\psi_v}{\partial u_p(\mathbf{q}_1)}\Big| P_c \frac{\partial H}{\partial u_{p'}(\mathbf{q}_2)} P_c \Big| \frac{\partial\psi_v}{\partial u_{p''}(\mathbf{q}_3)}\Big\rangle - \sum_{vv'} \Big\langle \frac{\partial\psi_v}{\partial u_p(\mathbf{q}_1)}\Big| P_c \Big| \frac{\partial\psi_{v'}}{\partial u_{p'}(\mathbf{q}_2)}\Big\rangle \langle\psi_{v'}| \frac{\partial H}{\partial u_{p''}(\mathbf{q}_3)}|\psi_v\rangle \\
&+\frac{1}{2}\int \frac{\partial^2 V_{ion}(\mathbf{r})}{\partial u_{p'}(\mathbf{q}_2)\partial u_{p''}(\mathbf{q}_3)} \frac{\partial n(\mathbf{r})}{\partial u_p(\mathbf{q}_1)} d\mathbf{r} + \frac{1}{6}\int \frac{\partial^3 V_{ion}(\mathbf{r})}{\partial u_p(\mathbf{q}_1)\partial u_{p'}(\mathbf{q}_2)\partial u_{p''}(\mathbf{q}_3)} n(\mathbf{r}) d\mathbf{r} \\
&\qquad +\frac{1}{6}\int \frac{\delta^3 E_{xc}[n]}{\delta n(\mathbf{r})\delta n(\mathbf{r}')\delta n(\mathbf{r}'')} \frac{\partial n(\mathbf{r})}{\partial u_p(\mathbf{q}_1)} \frac{\partial n(\mathbf{r}')}{\partial u_{p'}(\mathbf{q}_2)} \frac{\partial n(\mathbf{r}'')}{\partial u_{p''}(\mathbf{q}_3)} d\mathbf{r} d\mathbf{r}' d\mathbf{r}'',
\end{aligned} \tag{4.9}$$

where H and $|\psi_v\rangle$ are respectively the unperturbed self-consistent Hamiltonian and the corresponding wavefunctions, and $V_{ion}(\mathbf{r})$ is the *bare* (pseudo) potential acting on the electrons:

$$V_{ion}(\mathbf{r}) = \sum_{\mathbf{R},s} v_s(\mathbf{r} - \mathbf{R} - \tau_s),$$

v_s being the bare (pseudo) potential centered at atomic side $\mathbf{R} + \tau$. From Eq. 3.26 we finally obtain the expression for the dynamical tensor

$$\begin{aligned}
C_{pp'p''}(\mathbf{q}_1,\mathbf{q}_2,\mathbf{q}_3) &= \tilde{E}_{pp'p''}(\mathbf{q}_1,\mathbf{q}_2,\mathbf{q}_3) + \tilde{E}_{p'pp''}(\mathbf{q}_2,\mathbf{q}_1,\mathbf{q}_3) + \\
&+ \tilde{E}_{pp''p'}(\mathbf{q}_1,\mathbf{q}_3,\mathbf{q}_2) + \tilde{E}_{p''pp'}(\mathbf{q}_3,\mathbf{q}_1,\mathbf{q}_2) + \\
&+ \tilde{E}_{p'p''p}(\mathbf{q}_2,\mathbf{q}_3,\mathbf{q}_1) + \tilde{E}_{p''p'p}(\mathbf{q}_3,\mathbf{q}_2,\mathbf{q}_1),
\end{aligned} \tag{4.10}$$

So all ingredients necessary to compute the phonon linewidth are provided.

4.2 Technicalities

Simple semiconductors such as Silicon and Germanium crystallize in the diamond structure: the Bravais lattice is face-centered cubic with the two atoms per unit cell placed at $\tau_1 = 0$ and $\tau_2 = \frac{a}{4}(1,1,1)$, where a is the edge of the cube. For a given configuration of the nuclei, we have assumed that the electrons are in the corresponding ground state (adiabatic approximation).

Calculations were performed within density-functional theory in the local-density approximation for exchange and correlation energy. The input data for this approximation are the homogeneous electron gas exchange-correlation energy calculated with technique by Ceperley and Alder [34], and interpolated by Perdew and Zunger [35]. We have used the same norm-conserving pseudopotentials as in Ref. [21], which were generated using a scheme proposed by von Barth and Car [36]. Our plane-wave basis sets are truncated to a kinetic-energy cutoff of 22 Ry for Si and Ge and to 55 Ry for C, *i.e.* ~ 500 plane waves in both cases, which ensure a very accurate convergence in the third order force constants. The Brillouin-zone integration over electronic states is performed using the special point technique [37]. We have used the $(8,8,8)$ Monkhorst-Pack [32] integration mesh which reduces to the 10-point Chadi-Cohen set [37] in the irreducible wedge. Convergence tests for energy cutoff and for Monkhorst-Pack mesh are reported in appendix F. The reciprocal space integration over phonon states (the $\mathbf{q}$ points appearing in Eq. 2.8) was performed using the tetrahedron method, introduced by Lehemann and Taut [38] and independently by Jepsen and Andersen [39]. With this method we have performed the sum over the $\mathbf{q}$ points appearing in Eq. 2.8 using approximately 1500 tetrahedra in the irreducible wedge of the Brillouin zone to ensure a very accurate integration over the constant-energy surface given by Dirac's delta of Eq. 2.8. The integrand is calculated on a much coarser uniform mesh and then Fourier interpolated on the finer grid, much in the same way as phonon dispersions are obtained from selected calculations on a relatively coarse grid, passing through interatomic force constants [40]. Further details on the calculation are given in Appendix G.

Table 4.1: Calculated full widths at half maximum (2Γ) of zone-center optical phonons at zero temperature and pressure in C, Si and Ge. The corresponding experimental values are shown for comparison. The three last columns indicate the relative contributions of the individual decay channels (see text).

	2Γ (cm^{-1})	2Γ(expt) (cm^{-1})	LA+LA (%)	LA+TA (%)	TA+TA (%)
C	1.01	1.2[a]	14.7	33.9	30.7[b] + 20.7
Si	1.48	1.45[c]	6.0	94.0	-
Ge	0.67	0.66[d]	4.6	95.4	-

(a) From Ref.[13, f]. (b) *Klemens channel*, see text.
(c) From Ref.[43, c]. (d) From Ref.[6].

4.3 Numerical results

The calculated low-temperature linewidths of the LTO phonons in C, Si, and Ge are reported in Tab. 4.1 [41, 42], together with selected experimental data from Raman scattering and time resolved experiments. Although the spread in the published experimental results is rather large [13, 43, 44]—ranging from 1.2 to 2.9 cm^{-1} for C, from 1.24 to 2.1 cm^{-1} for Si, and from 0.66 to 1.4 cm^{-1} for Ge—we can conclude that the agreement is good.

To identify the relevant processes contributing to these results, in Tab. 4.1 we also report the relative weights of the individual decay channels, as obtained by restricting the sums over the j's in Eq. (1) to selected final states: 'TA' ($j = 1, 2$) and 'LA' ($j = 3$). The decay into one optical and one acoustic phonon is kinematically forbidden in all the present cases. It turns out that the dominant decay mechanisms are not the same in the three semiconductors. In Si and Ge, the process with maximum probability ($\simeq 95\%$) involves one LA and and one TA mode as final states, and the *Klemens channel*, i.e. the decay of the LTO mode into two acoustic phonons belonging to a same branch and with opposite momenta, turns out to give a very small contribution. In diamond, instead, the Klemens

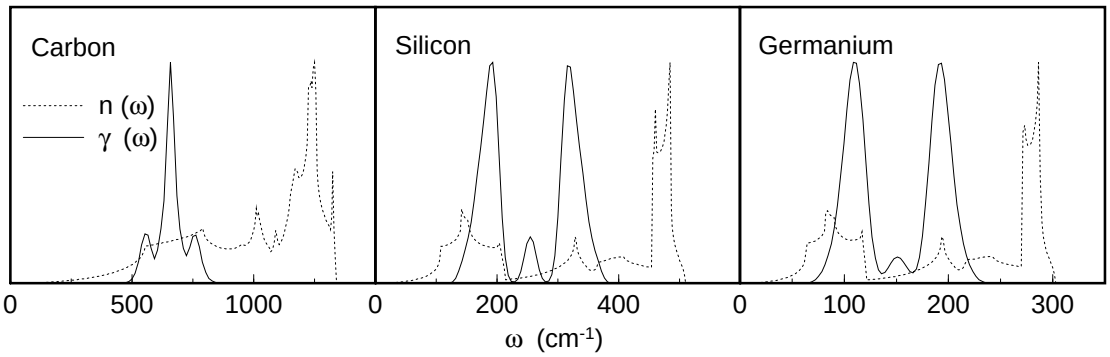

Figure 4.1: Calculated phonon density of states, $n(\omega)$ (solid line), and frequency-resolved final state spectra, $\gamma(\omega)$ (dashed line), for the three elemental semiconductors C, Si and Ge at zero temperature and pressure.

channels—TA+TA ($\simeq 31\%$) and LA+LA ($\simeq 15\%$)—become dominant at the expenses of the LA+TA channel. This analysis is made more clear by defining the *frequency-resolved final state spectrum*, $\gamma(\omega)$, i.e. the probability per unit time that the LTO phonon decays into one mode of given frequency ω and one of frequency $\omega_{LTO} - \omega$. In practice, $\gamma(\omega)$ is obtained by restricting the sum over j_1 and $\mathbf{q}$ in Eq. (1) to those values for which $\omega_{j_1}(\mathbf{q}) = \omega$, by inserting $\delta(\omega - \omega_{j_1}(\mathbf{q}))$ under the sign of sum. By its definition, $\gamma(\omega)$ is symmetric around $\omega_{LTO}/2$ and normalized to Γ. In Fig. 4.1 we display $\gamma(\omega)$, as calculated at $T = 0$ for the three materials considered here. The peak at $\omega_{LTO}/2$ corresponds to the Klemens decay mechanism. As anticipated in Tab. 4.1, this peak is dominant only in diamond. By comparison with the one-phonon density of states (DOS)—dashed lines in Fig. 4.1—, we realize that this occurs because diamond is the only case where $\omega_{LTO}/2$ falls in a region of relatively large DOS (between TA(L) and TA(X) [45]). For similar reasons the lateral peaks, symmetric with respect to $\omega_{LTO}/2$, are instead dominant for Si and Ge.

In order to get a deeper insight into the microscopic mechanisms which determine the decay process, we plot in Fig. 4.2 the *wavevector-resolved final state spectrum*, i.e. the $\mathbf{q}$-dependent function which appears in Eq. 2.8 under the sign of sum. Due to energy conservation, as expressed by the δ-function, this quantity is non zero only on a 3D surface of which we display the intersection with some high-symmetry planes in the Brillouin zone. The magnitude of the function on that surface (i.e. the magnitude of the matrix element

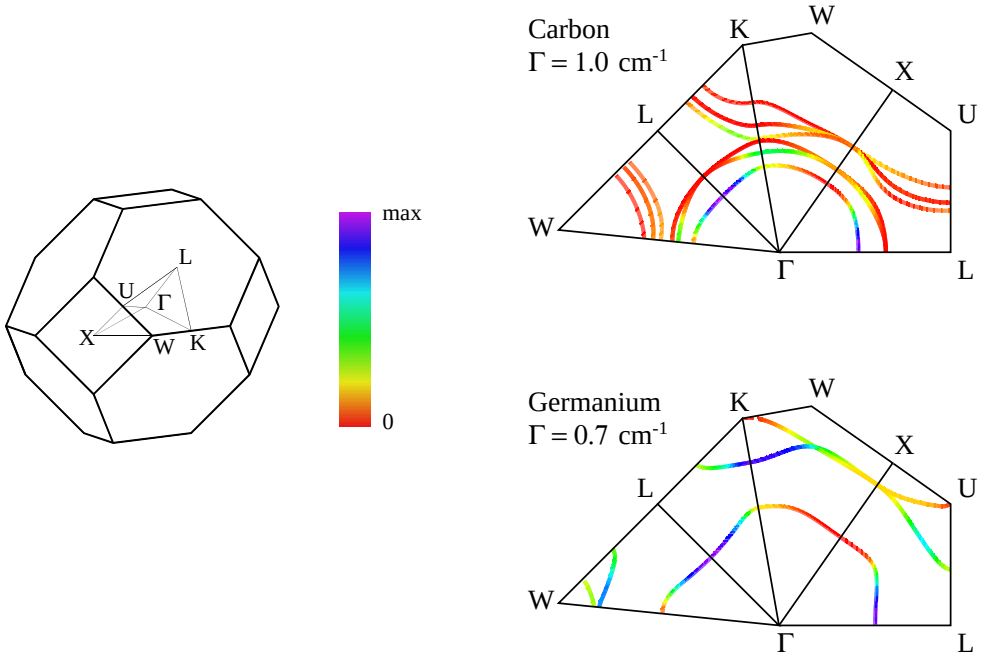

Figure 4.2: (color). Wavevector-resolved final-state spectra of C and Ge. The color scale goes from red to violet passing from the minimum to the maximum amplitude of each material. A sketch of the Brillouin zone is also displayed.

responsible for the phonon decay) is represented by a rainbow color scale going from red to violet in order of increasing magnitude. Let us examine diamond first. The inner line near Γ corresponds a $LA + LA$ to decay the other two nearby lines to a $LA + TA$ decay. The lines near the zone border instead correspond to decays into transverse acoustic modes. The wavevector-resolved final-state spectra of silicon and germanium are very similar (Si is shown in Fig. 4.5 together with its pressure dependence). Silicon and germanium display less decay channels than diamond, the line closer the Γ point corresponding to the decay process into the same LA branch the other two to $LA + TA$ decays.

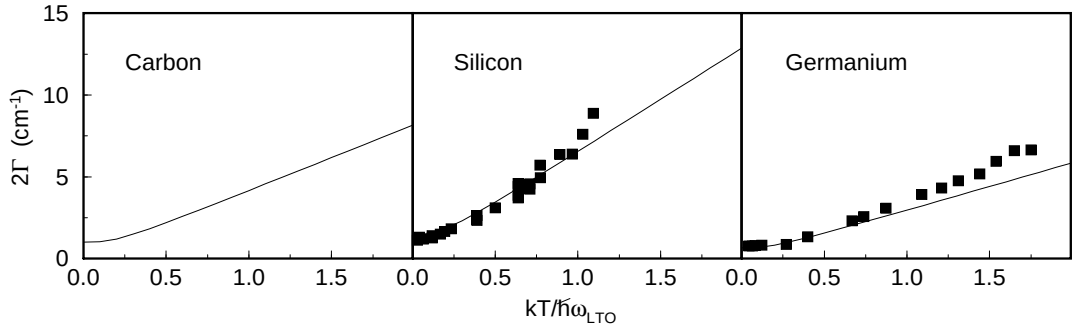

Figure 4.3: Temperature dependence of the full width at half maximum, 2Γ, of the LTO phonon in C, Si and Ge. Solid lines are the result of the present calculation; squares represent experimental data from Ref. [2].

4.3.1 Temperature dependence

In Fig. 4.3 we display the temperature dependence of the Raman linewidths in diamond, Si, and Ge, as obtained by including the appropriate thermal phonon occupation numbers in Eq. 2.8. The agreement is very good. The only deviations occur above $T \sim \hbar\omega_{LTO}/k_B$, i.e. far above room temperature, where higher-order anharmonic terms are likely to account for the discrepancies.

4.3.2 Pressure dependence

In Fig. 4.4 we report our predictions for the pressure dependence of the Raman linewidths, as obtained by performing calculations for different values of the crystal volume. For Si we have done calculations up to $P = 106$ Kbar, slightly below the observed transition pressure to the β-tin phase ($P^{tr} = 125 \pm 5$ Kbar, from Ref. [46]). For Ge, the results above 110 Kbar are not physical because a structural phase transition occurs at this pressure: the last two points are therefore of academic interest only and they were calculated for the sake of comparison with Silicon. The pressure dependence is relatively featureless for diamond, whereas it is characterized by a bimodal quasi-linear behavior for Si and Ge: the slope of the linewidth *vs.* pressure curve displays a rather well defined discontinuity at some critical pressures $P^\star$ ($P^\star \approx 70-80$, and $120-130$ Kbar, for Si and Ge respectively). This discontinuity can be understood in terms of the wavevector-resolved final state spectrum.

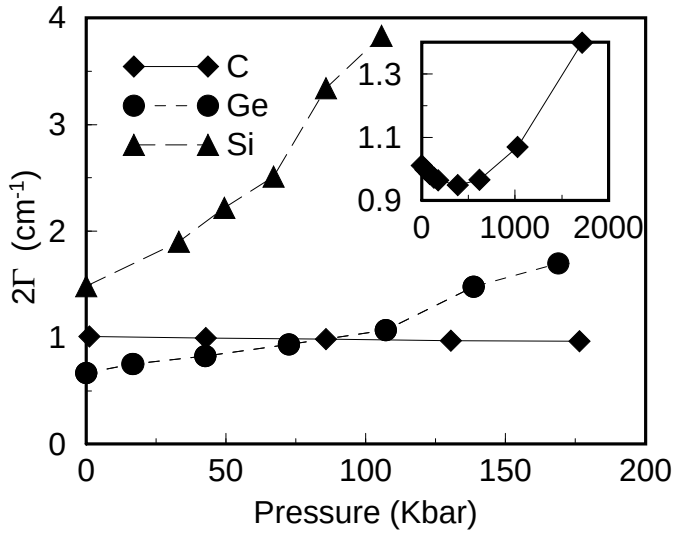

Figure 4.4: Calculated pressure dependence of the Raman linewidths (2Γ) for C, Si, and Ge in the diamond structure. The inset shows results over a larger pressure range for C. The lines are a guide for the eyes

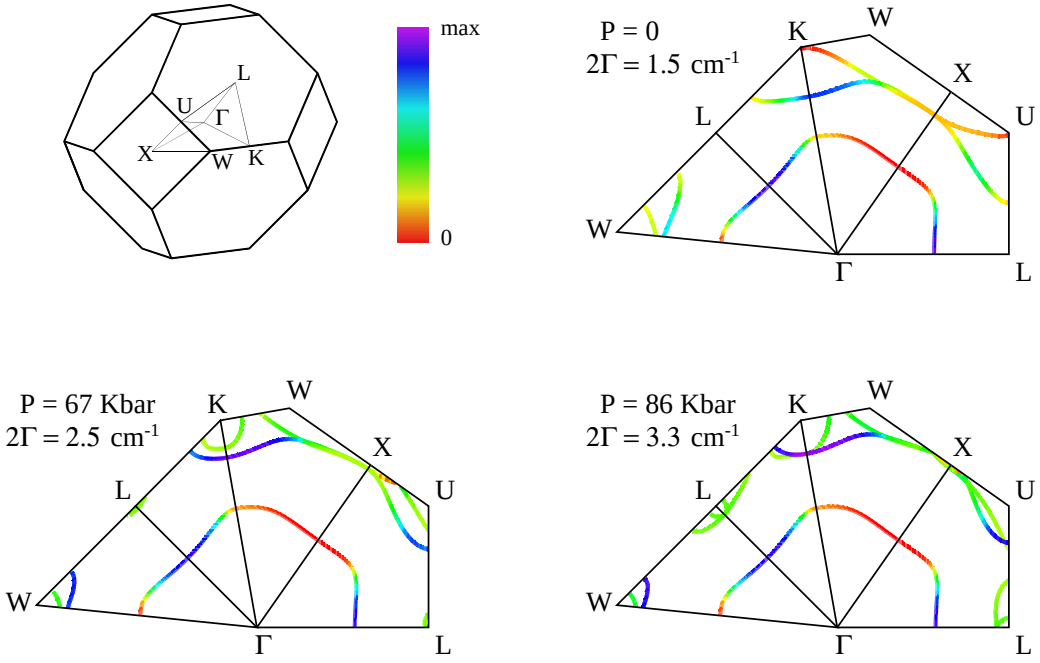

Figure 4.5: (color). Wavevector-resolved final-state spectra of Si (see text) at different pressures. (a) Sketch of the Brillouin zone; (b), (c) and (d) color maps at pressures $P = 0$, 67, 86 Kbar respectively. The color scale goes from red to violet in order of increasing magnitude.

Let us focus on Fig. 4.5(b) (zero pressure). It is easy to identify the contribution of Klemens processes in the closed contour falling approximately midway between the BZ center and edge (this is where the LA phonon dispersion $\omega_{LA}(\mathbf{q})$ reaches the value $\omega_{LA} = \omega_{LTO}/2$). The remaining contributions correspond to the LTO $\rightarrow$ LA+TA process, and come from wavevectors close to the BZ edge, in all the directions from Γ to zone boundary except around the $\Gamma - L$ direction, where the frequency of the TA branch is so low that no matching LA frequency exists yielding $\omega_{TA}(\mathbf{q}) + \omega_{LA}(-\mathbf{q}) = \omega_{LTO}$. A similar behavior is found also for Ge. The maps of Fig. 4(c) and 4(d) show that when the pressure increases, new channels begin to contribute, namely those related to regions of the Brillouin zone around the K and L points. The analysis of the corresponding final state spectra indicate that these channels involve LO and TA modes as final states, and are now compatible

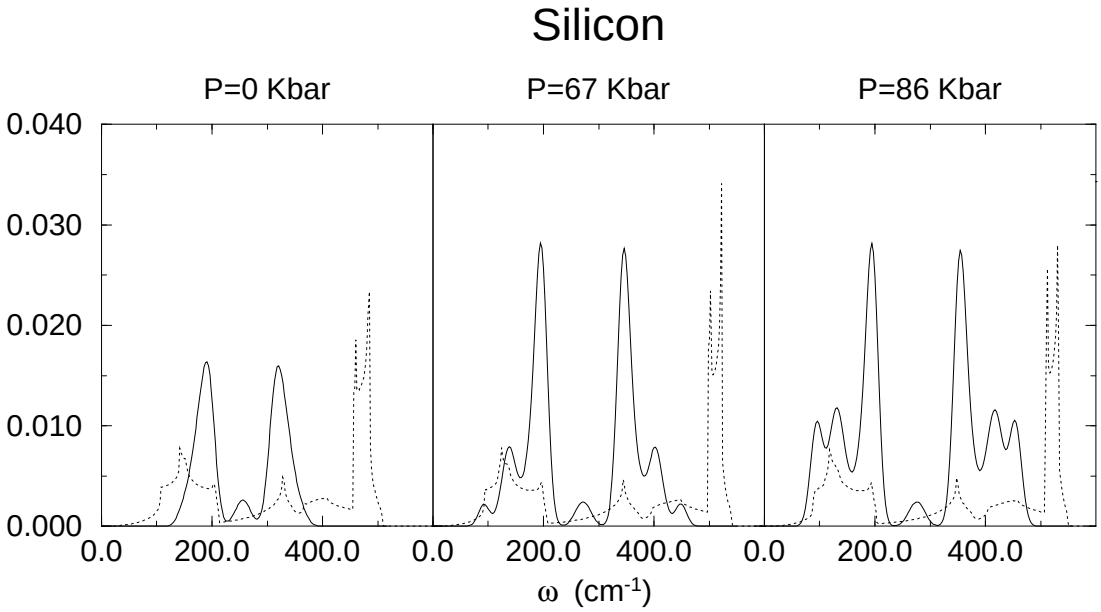

Figure 4.6: Calculated phonon density of states, $n(\omega)$ (solid line), and frequency-resolved final state spectra, $\gamma(\omega)$ (dashed line), for silicon at zero temperature and different pressure.

with energy conservation owing to two combined pressure-induced effects: the increased LTO frequency and the decreased frequency of the TA branches. We conclude that the dependence of the phonon lifetime upon pressure (and likely upon other applied fields as well) is quasi-linear as long as the overall kinematics does not change: when the applied field determines the opening of new decay channels otherwise closed, then a steep variation of the lifetime may occur.

These considerations are confirmed looking at the frequency-resolved final state spectra of Fig. 4.6. Around $P \sim 70$ Kbar two new peaks arise corresponding to the new decay channels into an optical and an acoustic mode. This decay channel is forbidden at zero pressure by energy conservation. In Tabs. 4.3.2, 4.3.2 and 4.3.2 we report the values obtained for the linewidths at various pressures in diamond, silicon and germanium respectively.

Table 4.2: Calculated full widths at half maximum (2Γ) of zone-center optical phonons at zero temperature for Diamond.

Pressure (Kbar)	2Γ (cm^{-1})	LA+LA (%)	TA+TA (%)	LA+TA (%)
0	1.01	14.7	30.7[a] + 20.7	33.9
620	0.97	10.0	37.5[a] + 20.5	32.0
1030	1.07	7.4	43.4[a] + 19.9	29.3
1720	1.40	4.4	48.3[a] + 23.0	24.3

[a] *Klemens channel*, see text.

Table 4.3: Calculated full widths at half maximum (2Γ) of zone-center optical phonons at zero temperature for Silicon. The contribution TA+LO is decomposed in two different channels: the first is due to the decay into the LO band and into the TA band with lower energy ($TA^{(1)}$); the second is due to decay into the LO band and into the other TA band ($TA^{(2)}$). Note the different behavior in the plot when the $TA^{(2)}$ contribution becomes non zero.

Pressure (Kbar)	2Γ (cm^{-1})	LA+LA (%)	LA+TA (%)	$TA^{(1)}$+LO (%)	$TA^{(2)}$+LO (%)
0	1.48	6.0	94.0	-	-
33	1.90	4.5	95.5	-	-
50	2.22	3.8	89.9	6.3	-
67	2.51	3.3	79.3	17.4	-
86	3.34	2.5	60.0	36.3	1.2
106	3.83	2.2	49.6	45.6	2.6

Table 4.4: Calculated full widths at half maximum (2Γ) of zone-center optical phonons at zero temperature for Germanium. The contribution TA+LO is decomposed in two different channels: the first is due to the decay into the LO band and into the TA band with lower energy ($TA^{(1)}$); the second is due to decay into the LO band and into the other TA band ($TA^{(2)}$). Note the different behavior in the plot when the $TA^{(2)}$ contribution becomes non zero.

Pressure (Kbar)	2Γ (cm^{-1})	LA+LA (%)	LA+TA (%)	$TA^{(1)}$ +LO (%)	$TA^{(2)}$+LO (%)
0	0.67	4.6	95.4	-	-
17	0.75	3.9	96.1	-	-
43	0.83	3.4	96.6	-	-
73	0.94	2.9	87.2	9.9	-
107	1.07	2.5	73.3	23.7	0.5
139	1.48	1.8	47.6	48.4	2.2
169	1.70	1.6	37.2	56.3	4.9

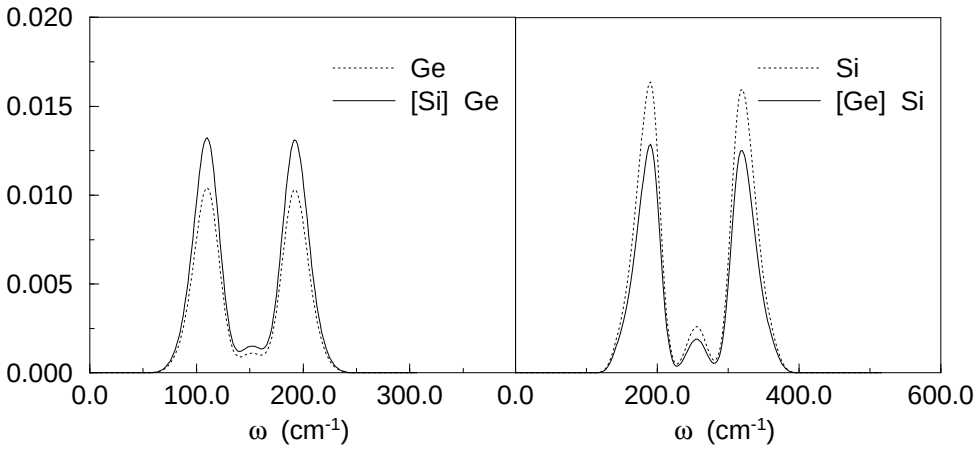

Figure 4.7: Comparison between frequency-resolved final state spectra, with (full line) and without (dotted line) mass approximation. [A] B means that the spectra of material B where obtained using the dynamical tensor of material A.

4.3.3 Mass approximation

The detailed numerical values of the phonon lifetime depend both on *kinematic* effects (i.e. on the existence of allowed decay channels) and on *dynamic* effects (i.e. on the magnitude of the matrix elements responsible for the instability of one-phonon states). The latter are given by the tensor of the third derivatives of the crystal energy with respect to atomic displacements. In order to assess the sensitivity of our results to an accurate evaluation of this tensor, we have performed test calculations of the linewidths of Si and Ge by interchanging their third-order coupling coefficients while leaving the kinematics (i.e. the phonon dispersion) unchanged. In spite of the similarities between the two materials, the results are affected by as much as 25%. We conclude that an accurate determination of the third-order anharmonic tensor is in general needed for a quantitative prediction of the lifetimes. For a quantitative comparison of third order force constant of Si and Ge see Appendix G (Tab. G.3)

5 Polar semiconductors

Polar semiconductors differ from the elemental ones studied in the previous chapter because they have two different atoms in the unit cell. The displacement of the atoms due to a longitudinal optical phonon at zone center may induce an electric field with the same wave-vector of the phonon; in semiconductors this electric field is not completely screened by electrons and adds to the restoring force acting on ions, thus modifying the phonon frequencies. This determines the splitting of transverse and longitudinal optical modes at zone center, as observed in the phonon spectra of polar semiconductors.

The splitting of LO and TO frequencies can be predicted by the so called phenomenological theory due to Huang [47]. The presence of an electric field produced by the LO phonon determines a non-analytic contribution to the dynamical matrix at the center of the Brillouin zone, which is derived in Appendix H. This contribution was computed by Cochran and Cowley [48] for a ionic crystal of arbitrary symmetry and after rederived in a famous work by Pick, Cohen and Martin [49], using a microscopic theory.

In zincblende semiconductors the macroscopic electric field associated to the phonon displacement does not affect the frequencies of transverse phonons but only of longitudinal ones; similarly, at third order the calculation of transverse phonon lifetimes involves no non-analytical contribution in the anharmonic dynamical tensor, while the calculation of the LO-lifetimes requires considering the effects of macroscopic electric field.

The difference in the electron density response to a longitudinal and an optical phonon in the long wave-length limit was discussed by Resta [50] for cubic materials with two atoms per unit cell. He showed that the first order correction to the density produced by

a LO phonon can be written as

$$n^{(1)}_{LO} = n^{(1)}_{TO} - \frac{4\pi e Z^*}{\Omega \epsilon_\infty} n^{(1)}_E \tag{5.1}$$

where $n^{(1)}_{TO}$ is the change density respect to a TO mode, $n^{(1)}_E$ is the linear density response to an uniform electric field, Z^* the Born effective charges, $-`e$ the electron charge, Ω the unit cell volume and ϵ_∞ the hight-frequency (electronic) dielectric tensor. The last term in the rhs of Eq. 5.1 is the contribution due to the coupling of LO-phonon with the associated electric field and include all non-analytic terms. In this chapter we present our results for the decay time of TO-phonons and some preliminary result on LO-phonon lifetimes, computed neglecting the contribution due to $n^{(1)}_E$ (and the corresponding non-analytical contribution to the wave-function response) in the anharmonic dynamical tensor.

In a polar semiconductor the longitudinal optical phonon at the Brillouin zone center has a frequency larger than that of the transverse one. So the decay of a LO-phonon into a transverse optical phonon and an acoustic one may be kinematically allowed also at small $\mathbf{q}$. When $\mathbf{q}$ vanishes, the acoustic frequencies, which appear at the denominator of Eq. 2.8, also vanish; for this reason it is useful to compute the limit of the wave-vector resolved FWHM (the contribution appearing in Eq. 2.8 under the sign of sum), $\Gamma(\mathbf{q})$, for $\mathbf{q} \to 0$ when one or more acoustic branches are involved. In section 5.2 we will prove that the integrand in Eq. 2.8 presents no singularities. As a preliminary step we derive, in the next section, a relation which must be satisfied by the anharmonic force constants.

5.1 Third order sum rule

We consider the expansion of the energy in powers of the displacements from the equilibrium positions, Eq. 4.1. The total energy of the system does not change for a rigid translation of all the atoms in the system,

$$u^l_{s,\alpha} \to u^l_{s,\alpha} + d_\alpha .$$

Replacing in this expression the third order term 4.4, we obtain

$$\frac{1}{2} \sum_{ll'l'',ss's'',\alpha\beta\gamma} C_{ss's'',\alpha\beta\gamma}(l,l',l'') u^l_{s,\alpha} u^{l'}_{s',\beta} d_\gamma + \tag{5.2}$$

$$+\frac{1}{2}\sum_{ll'l'',ss's'',\alpha\beta\gamma} C_{ss's'',\alpha\beta\gamma}(l,l',l'')u^l_{s,\alpha}d_\beta d_\gamma \tag{5.3}$$

$$+\frac{1}{6}\sum_{ll'l'',ss's'',\alpha\beta\gamma} C_{ss's'',\alpha\beta\gamma}(l,l',l'')d_\alpha d_\beta d_\gamma = 0 \tag{5.4}$$

$$\tag{5.5}$$

where we have used symmetry relations such as

$$C_{ss's'',\alpha\beta\gamma}(l,l',l'') = C_{ss''s',\alpha\gamma\beta}(l,l'',l').$$

Because the displacements d are arbitrary, the three sums must vanish separately. From the first one we obtain the sum rule for the anharmonic force constants:

$$\sum_{l'',s''} C_{ss's'',\alpha\beta\gamma}(l,l',l'') = 0, \tag{5.6}$$

and analogous rules are obtained by permutating the indices. The sum rule obtained from the second and third terms in Eq. 5.5 involves the summation on two or three indices and are particular cases of the above equation.

5.2 Analytic limit

Let us consider a solid with a frozen-in phonon of small momentum $\mathbf{q}$, defined by the ionic displacements:

$$u^l_{s,\alpha} = u_{s,\alpha}(\mathbf{q})e^{i\mathbf{q}\cdot\mathbf{R}^l_s}.$$

We perform the usual decomposition [51]:

$$u_{s,\alpha}(\mathbf{q}) = u_\alpha(\mathbf{q}) + \delta_{s,\alpha}(\mathbf{q}),$$

where the first term is the displacement of the cell as a whole and the second term is a relative displacement. They are respectively called acoustic and optical components. In the limit of small $\mathbf{q}$, $u_\alpha(\mathbf{q})$ vanishes for optical modes and $\delta_{s,\alpha}(\mathbf{q})$ vanishes for acoustic modes. Expanding the phonon displacement with respect to the wavevector up to first order in $\mathbf{q}$, we have for the acoustic component:

$$u_\alpha(\mathbf{q}) = u_\alpha + \sum_\beta u_{\alpha,\beta}q_\beta, \tag{5.7}$$

while the optical component is:

$$\delta_{s,\alpha}(\mathbf{q}) = \delta^s_\alpha + \sum_\beta \delta^s_{\alpha,\beta} q_\beta, \tag{5.8}$$

with the condition

$$\sum_s M_s \delta^s_\alpha = 0. \tag{5.9}$$

The frequency of a phonon in the j-th branch is

$$\omega_j(\mathbf{q}) = c_j\, q + \mathcal{O}(q^2) \tag{5.10}$$

for acoustic modes and

$$\omega_j(\mathbf{q}) = \omega_0 + \mathcal{O}(q^2) \tag{5.11}$$

for optical modes. We now consider the acoustic phonon $\mathbf{u}(\mathbf{q}, j_1)$ in the long-wave-length limit:

$$u_{s,\alpha}(\mathbf{q}) = u_\alpha + \sum_\beta u^s_{\alpha,\beta} q_\beta, \tag{5.12}$$

where the dependence on atomic position s is only in the term linear in $\mathbf{q}$ (which includes the eventual linear contribution of the optical component). From Eq. 2.8 we have that the linewidth of an optical phonon is proportional to the squared modulus of

$$\sum_{ss's'',\alpha\beta\gamma,l',l''} C_{ss's'',\alpha\beta\gamma}(l,l',l'') e_{s,\alpha}(\mathbf{0}, LTO) e_{s'',\beta}(\mathbf{q}, j_1) e_{s'',\gamma}(\mathbf{q}, j_2) e^{-i\mathbf{q}\cdot(\mathbf{R}^{l'} - \mathbf{R}^{l''})}. \tag{5.13}$$

Consider the case in which the decay process involve only one acoustic phonon. Inserting the expansion 5.12 in the numerator of Eq. 5.13 and expanding the exponential we obtain

$$\begin{aligned}
&\sum_{ss's'',\alpha\beta\gamma,l',l''} C_{ss's'',\alpha\beta\gamma}(l,l',l'') e_{s,\alpha}(\mathbf{0}, LTO) e_{s',\beta}(\mathbf{q}, j_1) e_{s'',\gamma}(-\mathbf{q}, j_2) e^{-i\mathbf{q}\cdot(\mathbf{R}^{l'} - \mathbf{R}^{l''})} = \\
&\sum_{ss's'',\alpha\beta\gamma,l',l''} \Big[C_{ss's'',\alpha\beta\gamma}(l,l',l'') e_{s,\alpha}(\mathbf{0}, LTO) e_\beta(j_1) e_{s'',\gamma}(-\mathbf{q}, j_2) + \\
&C_{ss's'',\alpha\beta\gamma}(l,l',l'') e_{s,\alpha}(\mathbf{0}, LTO) e_{\beta,\beta'}(j_1) q_{\beta'} e_{s'',\gamma}(-\mathbf{q}, j_2) \Big] e^{-i\mathbf{q}\cdot(\mathbf{R}^{l'} - \mathbf{R}^{l''})}
\end{aligned} \tag{5.14}$$

By expanding the exponential we find that the lowest order term in the right hand side contains the sum:

$$\sum_{l',s'} C_{ss's'',\alpha\beta\gamma}(l,l',l'') e_\beta(j_1) = 0, \tag{5.15}$$

where we have used the sum rule Eq. 5.6. It is easy to see that the remaining terms vanish linearly in $\mathbf{q}$. With the help of Eq. 5.10 and Eq. 5.11 we obtain after some straightforward algebra that:

$$\Gamma(\mathbf{q})_{\mathrm{LTO}\rightarrow\mathrm{LTA+LTO}} \propto q.$$

i.e. the contribution to linewidth due to decay process of LTO-phonon at BZ center into the LTA-phonon at $\mathbf{q}$ and into the LTO-phonon at $-\mathbf{q}$, must vanish linearly in q in the long-wave-length limit. In a similar way we can prove that:

$$\Gamma(\mathbf{q})_{\mathrm{LTO}\rightarrow\mathrm{LTA+LTA}} \propto q^2,$$

i.e. the decay process involving two acoustic bands must vanish quadratically for $\mathbf{q} \rightarrow 0$. It is easy to generalize these formulas to decay processes involving three different $\mathbf{q}$'s and one or more acoustic branches.

5.3 Results for polar semiconductors

In the following we present some preliminary results we have obtained for a few III-V semiconductors. The LO and TO decay processes are *kinematically different*: as discussed previously in a polar semiconductor the LO and TO branches are nondegenerate a $\mathbf{q} = 0$, so energy conservation allows different decay processes with the creation of phonons in different regions of the Brillouin zone. As it was previously pointed out the LO and TO decay processes are also *dynamically different*: due to the coupling with the electric field, a LO phonon induces a different density response than a transverse one. As a consequence the dynamical tensors corresponding to LO and TO phonons are different.

We have not yet implemented the calculation of the contribution of macroscopic electric fields to the lifetimes of LO-phonons, and we have so far neglected these contributions. Our results should be therefore considered exact within the LDA for TO phonons, while they are approximate for LO ones. The technical ingredients are the same used for simple semiconductors.

Table 5.1: Calculated full widths at half maximum (2Γ) of zone-center transverse optical phonons at zero temperature. The corresponding experimental values are shown for comparison. The last columns indicate the relative contributions to the linewidth of the individual decay channels (see text).

	2Γ (cm^{-1})	2Γ(expt) (cm^{-1})	LA+LA (%)	LA+TA (%)
GaAs	0.44	-	4.5	95.5
GaP	2.97	3.06[a]	2.3	97.1
AlAs	0.13	-	100.	-

(a) From Ref.[52].

5.3.1 Lifetime of TO-phonons

In Tab. 5.1 we report our results for the linewidths of transverse optical phonons at zero temperature. To the best of our knowledge the only experimental data available in the literature at low temperature are due to Bairamov, Kitaev, Negoduiko and Khashkhozhev (BKNK) for GaP [52]. The agreement between experimental data and our results is very good.

In Fig. 5.1 we plot the wavevector-resolved final-state spectra defined in Section 4.3. In GaAs and GaP the relevant contribution to the linewidth of TO-phonons is due to the decay into a longitudinal and a transverse acoustic phonon. GaP shows a large value of the linewidth compared to the values obtained for the other materials. In particular, in GaP the main contribution corresponds to the decay of TO $\rightarrow$ LA+TA phonons around the K-point.

5.3.2 Lifetime of LO-phonons

Our results for LO-phonons are shown in Tab. 5.2. In GaAs we compute $2\Gamma_{LO} = 0.66\,\mathrm{cm}^{-1}$; this value must be compared with the experimental datum $\tau = 9.2 \pm 0.6$ ps at $6K$ which correspond to $2\Gamma_{LO} = 0.58\,\mathrm{cm}^{-1}$, as was obtained by Vallée and Bogani

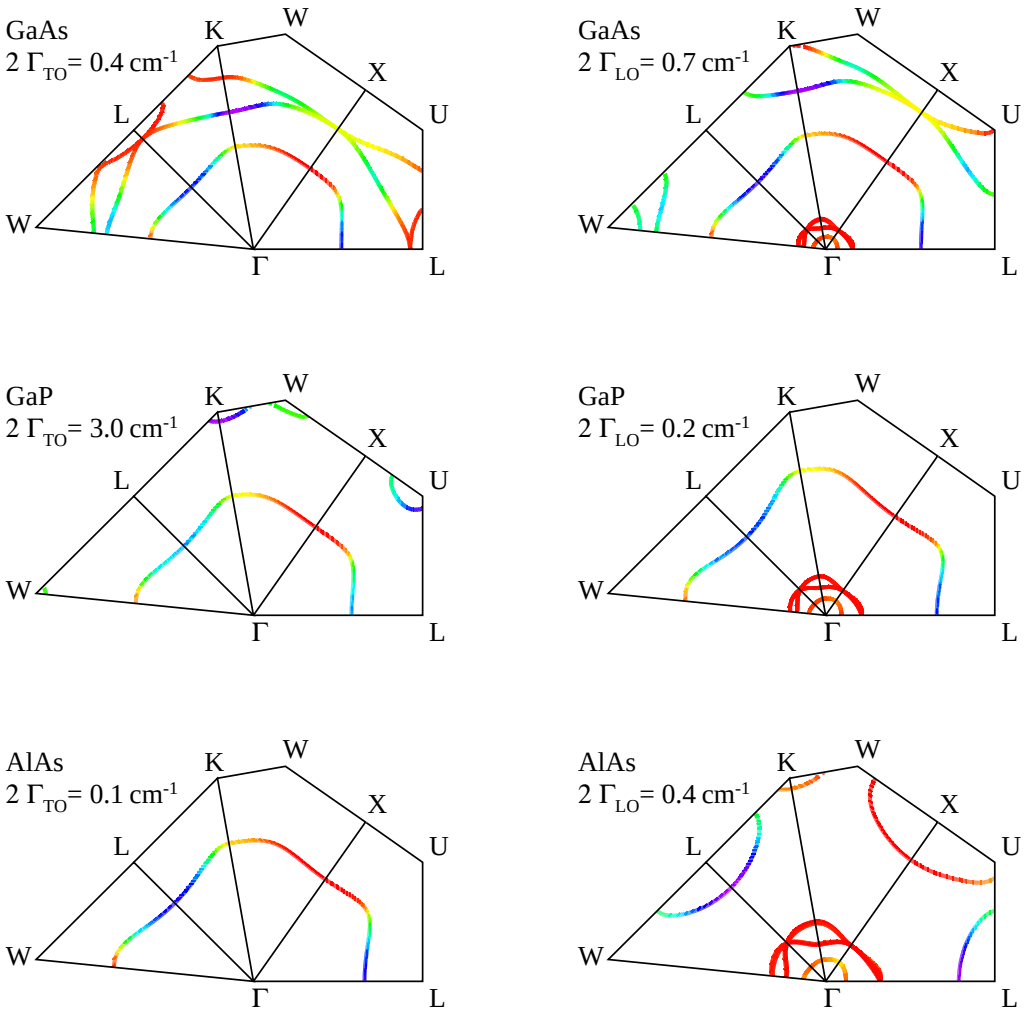

Figure 5.1: (color). Wavevector-resolved final-state spectra of polar material. The color scale goes from red to violet as in Fig. 4.5. In each material, violet corresponds to the maximum contribution on the constant energy surface.

Table 5.2: Calculated full widths at half maximum (2Γ) of zone-center longitudinal optical phonons at zero temperature and pressure. The corresponding experimental values are shown for comparison. The last columns indicate the relative contributions to the linewidth of the individual decay channels (see text).

	2Γ (cm^{-1})	2Γ(expt) (cm^{-1})	LA+LA (%)	LA+TA (%)	TO+LTA (%)
GaAs	0.66	0.58 ± 0.04^a	4.0	96.0	-
GaP	0.18	0.20 ± 0.02^b	96.0	-	4.0
AlAs	0.42	-	94.8	-	5.2

(a) From Ref.[53].

(b) From Ref.[8].

(VB) [53] using an infrared time-resolved coherent anti-Stokes Raman scattering (CARS) technique. In GaP we have computed a LO-phonon linewidth $2\Gamma_{LO} = 0.18\,\mathrm{cm}^{-1}$. The lifetime was measured by Bron, Kuhl and Rhee (BKR) [7, 8]; using CARS technique they found $\tau = 26.0 \pm 2.5$ ps. (at 5 K) which corresponds to $2\Gamma_{LO} = 0.20 \pm 0.02\,\mathrm{cm}^{-1}$. They also measured the linewidth by spontaneous Raman scattering intensity and found $2\Gamma_{LO} = 0.23\,\mathrm{cm}^{-1}$. A previous measurement of LO-phonon linewidth was obtained by Bairamov *et al.* [52]; at 15.K they found $2\Gamma_{LO} = 0.36 \pm 0.02\,\mathrm{cm}^{-1}$. [1]

With the help of Tab. 5.2 and Fig. 5.1 we can pinpoint the relevant LO decay processes. The red lines around the Γ-point refer to the decay channels LO $\rightarrow$ TO+LA and LO $\rightarrow$ TO+TA which give a negligible contribution to the linewidth according to the results of section 5.2 (it is zero in GaAs where the allowed decay processes involve q-points closer to the Γ-point, a few percents in the other materials). The decay of the LO phonon in GaAs shows mechanisms similar to those found in Si and Ge (see Fig. 4.5). The most important decay mechanism involve two different branches: LA+TA. These processes correspond to the colored lines near the boundaries of the Brillouin zone in Fig. 5.1. In GaP and AlAs

[1] Note that in Bairamov's work the instrumental linewidth was of 0.14 cm^{-1}, it is comparable with the linewidth measured. See Fig.2 of Ref. [52]

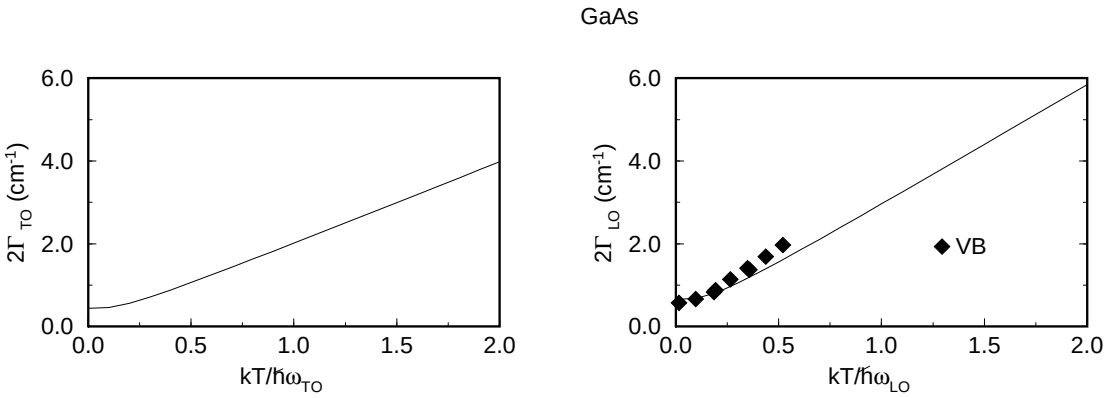

Figure 5.2: Temperature dependence of the full width at half maximum, 2Γ, of the TO and LO phonons in GaAs. Diamonds denote experimental data from Ref. [53].

the relevant mechanism is the decay into the same longitudinal acoustical branch, as it is shown in the figure by the blue line around the L-point.

5.4 Temperature dependence

We have computed the temperature dependence of linewidth for transverse and longitudinal optical phonons. Our results are shown in Fig. 5.2, 5.3, 5.4 for GaAs, GaP and AlAs respectively; the continuous line is our theoretical results, the experimental data are denoted by symbols. The experimental data for $2\Gamma_{LO}$ in GaAs are due to Vallée and Bogani [53]. For completeness, we mention the earlier experimental data obtained by von der Linde *et al.* [9] at 77 K. for the phonon lifetime of LO-mode in GaAs. They have measured the time evolution of non-equilibrium incoherent optical phonons, finding $2\Gamma_{LO} = 0.76\,\mathrm{cm}^{-1}$. At the same temperature they also measured the LO-phonon Raman linewidth $2\Gamma_{LO} = 0.85 \pm 0.1\,\mathrm{cm}^{-}1$. At 77 K. Vallée *et al.* obtain $2\Gamma_{LO} = 0.83 \pm 0.05\,\mathrm{cm}^{-1}$i, in very good agreement with our result of $2\Gamma_{LO} = 0.81\ \mathrm{cm}^{-1}$.

In GaP our result for $2\Gamma_{TO}$ shows a strong temperature dependence (it changes by a order of magnitude in the temperature range considered). Our results are in good agreement with available experimental data only at low temperature. In our opinion the

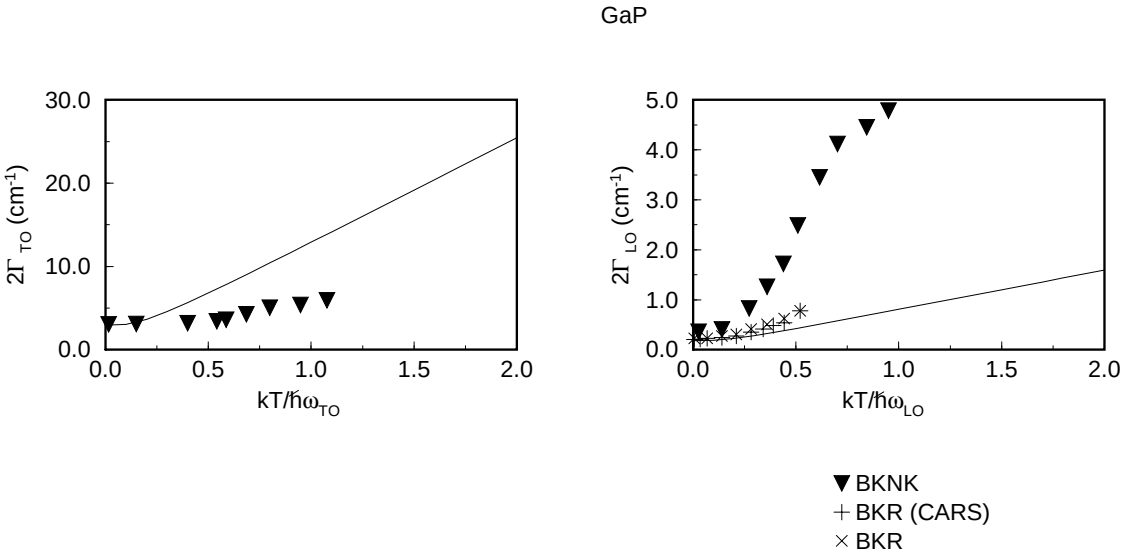

Figure 5.3: Temperature dependence of the full width at half maximum, 2Γ, of the TO and LO phonons in GaP. Solid lines are the result of the present calculation; triangles represent experimental data from Ref. [52]; + and × denote experimental data obtained by CARS and Raman width respectively, from Ref. [7].

discrepancies between theory and experiment may be explained by the observation that the relevant contribution in the computation Γ_{TO} comes from decay processes in a small surface around the K-point. The contribution to the linewidth due to this particular a decay mechanism can be sensitively modified, also at small temperature, by the high order contribution neglected in our computation.

The temperature dependence of $2\Gamma_{LO}$ in GaP is reported in Fig. 5.3. Our calculation is in good agreement with BKR experimental data, up to room temperature when the higher order corrections are expected to become important.

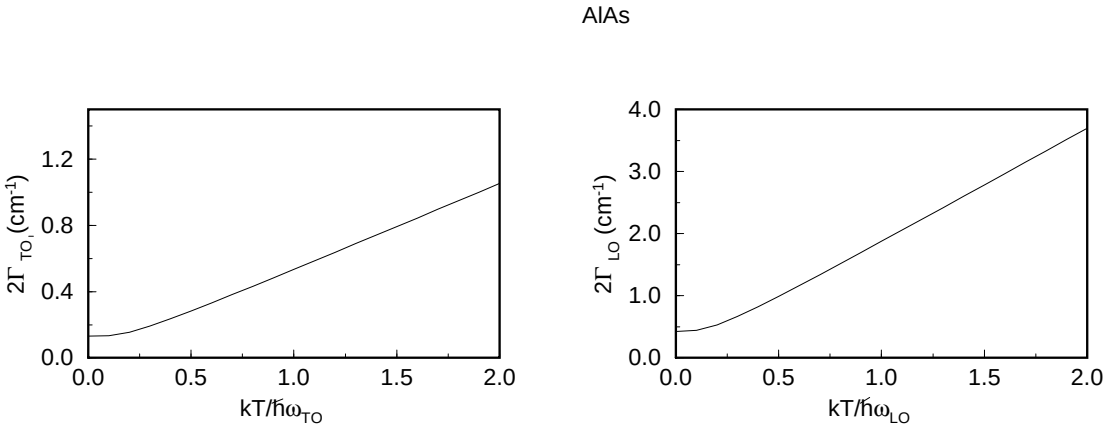

Figure 5.4: Temperature dependence of the full width at half maximum, 2Γ, of the TO and LO phonons in AlAs.

6 Conclusions

In this thesis we have presented the first *ab initio* calculation of anharmonic effects in crystals. The crucial step has been an efficient implementation of third order density-functional perturbation theory.

Our formulation can be used to compute all the physical quantities which are third derivatives of to the electronic energy of the system with respect to some external perturbations. Among them we have focused our attention on the phonon lifetimes: a relatively large amount of experimental data was not satisfactorily explained by previous theoretical work, due to the difficulties to provide reliable theoretical models to describe the kinematics and the dynamics of the decay processes.

Our results show that first principles calculations of third-order interactions provide an accurate description of the anharmonic decay of phonons in semiconductors at zero temperature both in simple (diamond structure) and in polar (zincblende structure) semiconductors. In general, our computed temperature dependent phonon lifetimes are in good agreement with experimental data up to and slightly above room temperature. The only exception is the TO-lifetime of GaP, which require of further theoretical and experimental investigation.

The study of the pressure dependence has provided reliable predictions where the experimental data lack. Our calculation of decay time in Si under pressure is a good example of how the activation of new decay channels driven by the pressure, can be analyzed with our technique. Different competing two-phonon decay channels are compared quantitatively and correlated to the density of final states.

The success of our computation is due to the fact that density functional perturbation

theory gives a very accurate description both of the kinematics and of the dynamics of the system.

In summary, our results are in excellent agreement with available experimental data and provide reliable predictions when the latter are lacking. Within density functional perturbation theory, the required computational effort is comparable to that needed by standard lattice-dynamical calculations in the harmonic approximation. This opens the way to the prediction of anharmonic lifetimes in systems—such as heterostructures—where they are not easily accessed by experiments, and to the study of modifications which can be induced by varying various applied fields and/or the characteristics of the samples by materials engineering.

Appendix A
The harmonic problem

In this appendix we describe how compute the phonon frequencies and displacements, introducing the relative notation. As we have seen in Chapter 2 up to second order the Taylor expansion of the energy gives:

$$E_{tot}(\{\mathbf{u}_s^l\}) = E_{tot}^{(0)} + \frac{1}{2}\sum_{ll',ss',\alpha\beta} C_{ss',\alpha\beta}(l,l')u_{s,\alpha}^{l}u_{s',\beta}^{l'} \tag{A.1}$$

Differentiation of this equation with respect to $u_{s,\alpha}^l$ gives the α component of the force acting on the atom on side $\mathbf{R}_s^l$

$$F_\alpha(\mathbf{R}_s^l) = -\frac{\partial E_{tot}}{\partial u_{s,\alpha}^l} = -\sum_{l',s',\beta} C_{ss',\alpha\beta}(l,l')u_{s',\beta}^{l'} \tag{A.2}$$

Not all of the force constants are independent: they are related by the symmetry operations of the system. In particular, because of translational invariance, the harmonic force constants only depend on the difference $\mathbf{R}_s^l - \mathbf{R}_{s'}^{l'}$. Because the force acting on an atom must be unchanged if we translate the system as a whole. This implies that the force constants must satisfy the relation:

$$\sum_{l',s'} C_{ss',\alpha\beta}(l,l') = 0. \tag{A.3}$$

Using the classical equation of motion we have, from Eq. A.2:

$$M_s\ddot{u}_{\alpha,s}^l = -\sum_{l',s',\beta} C_{ss',\alpha\beta}(l,l')u_{s',\beta}^{l'}. \tag{A.4}$$

In view of the periodicity of the lattice, we seek the solution of this equation in the form of a traveling wave,

$$\mathbf{u}_s^l = \mathbf{u}_s(\mathbf{q})e^{i\mathbf{q}\cdot\mathbf{R}^l - i\omega t} \tag{A.5}$$

Substituting this expression into Eq. A.4 we obtain:

$$\omega^2 M_s u_{\alpha,s}(\mathbf{q}) = \sum_{s',\beta} C_{ss',\alpha\beta}(\mathbf{q}) u_{s',\beta}(\mathbf{q}) \tag{A.6}$$

where we have defined the dynamical matrix

$$C_{ss',\alpha\beta}(\mathbf{q}) = \sum_{l,l'} C_{ss',\alpha\beta}(l,l') e^{-i\mathbf{q}\cdot(\mathbf{R}^l - \mathbf{R}^l)} \tag{A.7}$$

which is a $3n \times 3n$ hermitian matrix. From Eq. A.5, remembering that force constants defined in Eq. 4.3 are real and do not depend of the order of differentiation, we have can derive that

$$C_{ss',\alpha\beta}(-\mathbf{q}) = C^*_{ss',\alpha\beta}(\mathbf{q}) = C_{s's,\beta\alpha}(\mathbf{q}) \tag{A.8}$$

Introducing the scaled quantities:

$$e_{s,\alpha}(\mathbf{q}) \equiv \sqrt{M_s} u_{s,\alpha}(\mathbf{q}),$$

we rewrite equation A.6 as

$$\omega^2 e_{\alpha,s}(\mathbf{q}) = \sum_{s',\beta} \frac{C_{ss',\alpha\beta}(\mathbf{q})}{\sqrt{M_s M_{s'}}} e_{s',\beta}(\mathbf{q}). \tag{A.9}$$

Diagonalization of Eq. A.9 gives the phonon frequencies $\omega_j(\mathbf{q})$ and the phonon displacements $e_{s,\alpha}(\mathbf{q},j)$, where $j = 1,\cdots,3n$ labels the phonon branches. Note that we have adopted the usual normalization:

$$\sum_{s,\alpha} e^*_{s,\alpha}(\mathbf{q},j) e_{s,\alpha}(\mathbf{q},j') = \delta_{j,j'} \tag{A.10}$$

Appendix B
The "$2n+1$" theorem

Following the demonstration by Gonze and Vigneron [17] we perform the perturbative expansion of the quantities and equations we have defined in Chapter 3, as a function of the small parameter λ:

$$H(\lambda) = H^{(0)} + \lambda H^{(1)} + \lambda^2 H^{(2)} + \lambda^3 H^{(3)} + \cdots$$

Introducing the quantity

$$\widetilde{H}_\alpha \equiv H - \epsilon_\alpha ,$$

we can write the Schrödinger equation and the normalization condition at order i in a more compact form

$$\sum_{j=0}^{i} \widetilde{H}_\alpha^{(j)} \left| \psi_\alpha^{(i-j)} \right\rangle = 0 \tag{B.1}$$

$$\sum_{j=0}^{i} \langle \psi_\alpha^{(j)} \left| \psi_\alpha^{(i-j)} \right\rangle = 0 \qquad i \neq 0$$

Let us consider the identity:

$$\langle \psi_\alpha | \, \widetilde{H}_\alpha \, | \psi_\alpha \rangle = 0$$

which can be expressed in terms of the perturbative expansion as

$$\sum_{j=0}^{i} \sum_{k=0}^{i} \left\langle \psi_\alpha^{(j)} \right| \widetilde{H}_\alpha^{(i-j-k)} \left| \psi_\alpha^{(k)} \right\rangle = 0$$

With this equation we can form triangular tables similar to the following one, associated to the third order terms:

$$\begin{aligned}
0 \;=\;& \langle\psi_\alpha^{(3)}|\,\widetilde{H}_\alpha^{(0)}\,|\psi_\alpha^{(0)}\rangle \\
+\;& \langle\psi_\alpha^{(2)}|\,\widetilde{H}_\alpha^{(1)}\,|\psi_\alpha^{(0)}\rangle + \langle\psi_\alpha^{(2)}|\,\widetilde{H}_\alpha^{(0)}\,|\psi_\alpha^{(1)}\rangle \\
+\;& \langle\psi_\alpha^{(1)}|\,\widetilde{H}_\alpha^{(2)}\,|\psi_\alpha^{(0)}\rangle + \langle\psi_\alpha^{(1)}|\,\widetilde{H}_\alpha^{(1)}\,|\psi_\alpha^{(1)}\rangle + \langle\psi_\alpha^{(1)}|\,\widetilde{H}_\alpha^{(0)}\,|\psi_\alpha^{(2)}\rangle \\
+\;& \langle\psi_\alpha^{(0)}|\,\widetilde{H}_\alpha^{(3)}\,|\psi_\alpha^{(0)}\rangle + \langle\psi_\alpha^{(0)}|\,\widetilde{H}_\alpha^{(2)}\,|\psi_\alpha^{(1)}\rangle + \langle\psi_\alpha^{(0)}|\,\widetilde{H}_\alpha^{(1)}\,|\psi_\alpha^{(2)}\rangle + \langle\psi_\alpha^{(0)}|\,\widetilde{H}_\alpha^{(0)}\,|\psi_\alpha^{(3)}\rangle
\end{aligned}$$

Using Eq. (B.1) one can see that the sum of the terms of any horizontal line vanishes, and the same holds for the sum of any vertical line. The first two lines and the last two columns as zero and can be eliminated; we can finally isolate $\epsilon_\alpha^{(3)}$:

$$\begin{aligned}
\epsilon_\alpha^{(3)} \;=\;& \left\langle\psi_\alpha^{(1)}\middle|H^{(2)}\middle|\psi_\alpha^{(0)}\right\rangle + \left\langle\psi_\alpha^{(1)}\middle|H^{(1)}-\epsilon_\alpha^{(1)}\middle|\psi_\alpha^{(1)}\right\rangle \\
+\;& \left\langle\psi_\alpha^{(0)}\middle|H^{(3)}\middle|\psi_\alpha^{(0)}\right\rangle + \left\langle\psi_\alpha^{(0)}\middle|H^{(2)}\middle|\psi_\alpha^{(1)}\right\rangle
\end{aligned} \tag{B.2}$$

This procedure may be generalized to a case of order i; one has to repeat the same construction by eliminating, in the corresponding "triangular table", the first m rows and the last m columns, where $m = [(i+1)/2]$ ($[k]$ denote the integer part of k). Explicit formulas valid at any order may be found in [17].

For a *non*-self-consistent perturbative hamiltonian, known at any order, one can show, using the previous construction, that the n-th order eigenfunctions give the eigenenergies up to the $(2n+1)$-st order. In the self-consistent case, however, the $H^{(i)}$ functionally depends on *all* the order j in the eigenfunctions with $j \leq i$:

$$H^{(i)} = v_{\text{ext}}^{(i)} + \left[\frac{\delta E_I\left[n^{(0)} + \sum_{j=1}^{i}\lambda^j\, n^{(j)}\right]}{\delta n(\mathbf{r})}\right]^{(i)}$$

$$n^{(i)}(\mathbf{r}) = \sum_\alpha \sum_{j=0}^{i} \psi_\alpha^{(j)*}(\mathbf{r})\,\psi_\alpha^{(i-j)}(\mathbf{r})$$

Nevertheless, an exact cancellation of terms occurs in the total energy expression Eq. (3.2), which restores the $2n+1$ theorem. We will demonstrate it for the third order terms of

the total energy. It is useful to introduce the following notation:

$$F^{(k)}(\mathbf{r}_1, \mathbf{r}_2, \ldots, \mathbf{r}_k) \equiv \frac{\delta^k E_I[n^{(0)}]}{\delta n(\mathbf{r}_1) \cdots \delta n(\mathbf{r}_k)} \tag{B.3}$$

Then, we consider the sum of the third-order eigenvalues given in Eq. (B.2):

$$\begin{aligned}
\sum_\alpha \epsilon_\alpha^{(3)} &= \sum_\alpha \left[\left\langle \psi_\alpha^{(1)} \right| v_{\mathrm{ext}}^{(2)} \left| \psi_\alpha^{(0)} \right\rangle + \left\langle \psi_\alpha^{(1)} \right| H^{(1)} - \epsilon_\alpha^{(1)} \left| \psi_\alpha^{(1)} \right\rangle \right. \\
&+ \left. \left\langle \psi_\alpha^{(0)} \right| v_{\mathrm{ext}}^{(3)} \left| \psi_\alpha^{(0)} \right\rangle + \left\langle \psi_\alpha^{(0)} \right| v_{\mathrm{ext}}^{(2)} \left| \psi_\alpha^{(1)} \right\rangle \right] \\
&+ \int F^{(2)}(\mathbf{r}, \mathbf{r}')\, n^{(2)}(\mathbf{r})\, n^{(1)}(\mathbf{r}')\, \mathrm{d}\mathbf{r}\, \mathrm{d}\mathbf{r}' \\
&+ \int F^{(2)}(\mathbf{r}, \mathbf{r}')\, n^{(3)}(\mathbf{r})\, n^{(0)}(\mathbf{r}')\, \mathrm{d}\mathbf{r}\, \mathrm{d}\mathbf{r}' \quad + \\
&+ \frac{1}{2} \int F^{(3)}(\mathbf{r}, \mathbf{r}', \mathbf{r}'')\, n^{(1)}(\mathbf{r})\, n^{(1)}(\mathbf{r}')\, n^{(1)}(\mathbf{r}'')\, \mathrm{d}\mathbf{r}\, \mathrm{d}\mathbf{r}'\, \mathrm{d}\mathbf{r}'' \\
&+ \int F^{(3)}(\mathbf{r}, \mathbf{r}', \mathbf{r}'')\, n^{(1)}(\mathbf{r})\, n^{(2)}(\mathbf{r}')\, n^{(0)}(\mathbf{r}'')\, \mathrm{d}\mathbf{r}\, \mathrm{d}\mathbf{r}'\, \mathrm{d}\mathbf{r}'' \\
&+ \frac{1}{6} \int F^{(4)}(\mathbf{r}, \mathbf{r}', \mathbf{r}'', \mathbf{r}''')\, n^{(1)}(\mathbf{r})\, n^{(1)}(\mathbf{r}')\, n^{(1)}(\mathbf{r}'')\, n^{(0)}(\mathbf{r}''')\, \mathrm{d}\mathbf{r}\, \mathrm{d}\mathbf{r}'\, \mathrm{d}\mathbf{r}''
\end{aligned}$$

The procedure is similar for the second part of Eq. (3.2):

$$\begin{aligned}
\left[\int \frac{\delta E_I[n]}{\delta n(\mathbf{r})}\, n(\mathbf{r})\, \mathrm{d}\mathbf{r} - E_I[n] \right]^{(3)} &= \\
&\int F^{(2)}(\mathbf{r}, \mathbf{r}')\, n^{(2)}(\mathbf{r})\, n^{(1)}(\mathbf{r}')\, \mathrm{d}\mathbf{r}\, \mathrm{d}\mathbf{r}' + \\
&\int F^{(2)}(\mathbf{r}, \mathbf{r}')\, n^{(3)}(\mathbf{r})\, n^{(0)}(\mathbf{r}')\, \mathrm{d}\mathbf{r}\, \mathrm{d}\mathbf{r}' + \\
&\frac{1}{3} \int F^{(3)}(\mathbf{r}, \mathbf{r}', \mathbf{r}'')\, n^{(1)}(\mathbf{r})\, n^{(1)}(\mathbf{r}')\, n^{(1)}(\mathbf{r}'')\, \mathrm{d}\mathbf{r}\, \mathrm{d}\mathbf{r}'\, \mathrm{d}\mathbf{r}'' + \\
&\int F^{(3)}(\mathbf{r}, \mathbf{r}', \mathbf{r}'')\, n^{(1)}(\mathbf{r})\, n^{(2)}(\mathbf{r}')\, n^{(0)}(\mathbf{r}'')\, \mathrm{d}\mathbf{r}\, \mathrm{d}\mathbf{r}'\, \mathrm{d}\mathbf{r}'' +
\end{aligned}$$

$$\frac{1}{6}\int F^{(4)}(\mathbf{r},\mathbf{r}',\mathbf{r}'',\mathbf{r}''')\,n^{(1)}(\mathbf{r})\,n^{(1)}(\mathbf{r}')\,n^{(1)}(\mathbf{r}'')\,n^{(0)}(\mathbf{r}''')\,\mathrm{d}\mathbf{r}\,\mathrm{d}\mathbf{r}'\,\mathrm{d}\mathbf{r}''$$

We finally obtain Eq. 3.17

$$\begin{aligned} E^{(3)} &= \sum_\alpha \left[\left\langle \psi_\alpha^{(1)} \right| v_{\mathrm{ext}}^{(2)} \left| \psi_\alpha^{(0)} \right\rangle + \left\langle \psi_\alpha^{(1)} \right| H^{(1)} - \epsilon_\alpha^{(1)} \left| \psi_\alpha^{(1)} \right\rangle \right. \\ &+ \left. \left\langle \psi_\alpha^{(0)} \right| v_{\mathrm{ext}}^{(3)} \left| \psi_\alpha^{(0)} \right\rangle + \left\langle \psi_\alpha^{(0)} \right| v_{\mathrm{ext}}^{(2)} \left| \psi_\alpha^{(1)} \right\rangle \right] \\ &+ \frac{1}{6}\int F^{(3)}(\mathbf{r},\mathbf{r}',\mathbf{r}'')\; n^{(1)}(\mathbf{r})\; n^{(1)}(\mathbf{r}')\; n^{(1)}(\mathbf{r}'')\; \mathrm{d}\mathbf{r}\,\mathrm{d}\mathbf{r}'\,\mathrm{d}\mathbf{r}'' \end{aligned} \tag{B.4}$$

an expression which shows no explicit dependence on the perturbative correction of the particle density and the KS eigenfunctions, except for the first-order terms. This is the demonstration of $2n+1$ theorem with $n=1$. The cancellation of high-order corrections is not restricted to the third-order expression. The first, third and fourth terms in Eq. B.4 can be easily rewritten (in the case of local external potential) in terms of $n^{(0)}$ and $n^{(1)}$ [51].

$$\sum_\alpha \left[\left\langle \psi_\alpha^{(1)} \right| v_{\mathrm{ext}}^{(2)} \left| \psi_\alpha^{(0)} \right\rangle + \left\langle \psi_\alpha^{(0)} \right| v_{\mathrm{ext}}^{(2)} \left| \psi_\alpha^{(1)} \right\rangle \right] = \int v_{\mathrm{ext}}^{(2)}(\mathbf{r}) n^{(1)}(\mathbf{r}) d\mathbf{r}.$$

$$\sum_\alpha \left[\left\langle \psi_\alpha^{(0)} \right| v_{\mathrm{ext}}^{(3)} \left| \psi_\alpha^{(0)} \right\rangle + \right] = \int v_{\mathrm{ext}}^{(3)}(\mathbf{r}) n^{(0)}(\mathbf{r}) d\mathbf{r}.$$

Using Eq.B.3 and Eq. 3.3 we obtain

$$\begin{aligned} E^{(3)} &= \sum_\alpha \left[\left\langle \psi_\alpha^{(1)} \right| H^{(1)} - \epsilon_\alpha^{(1)} \left| \psi_\alpha^{(1)} \right\rangle \right] \\ &+ \int v_{\mathrm{ext}}^{(2)}(\mathbf{r}) n^{(1)}(\mathbf{r}) d\mathbf{r} + \int v_{\mathrm{ext}}^{(3)}(\mathbf{r}) n^{(0)}(\mathbf{r}) d\mathbf{r} \\ &+ \frac{1}{6}\int \frac{\delta^3 E_{xc}[n]}{\delta n(\mathbf{r})\delta n(\mathbf{r}')\delta n(\mathbf{r}'')}\; n^{(1)}(\mathbf{r})\; n^{(1)}(\mathbf{r}')\; n^{(1)}(\mathbf{r}'')\; \mathrm{d}\mathbf{r}\,\mathrm{d}\mathbf{r}'\,\mathrm{d}\mathbf{r}''. \end{aligned} \tag{B.5}$$

Appendix C
Uniform electric field

When the perturbation is an uniform electric field Eq. 3.27 permits to compute the third order correction to the energy in solids, skipping the problem that the field $e\mathcal{E}\mathbf{r}$ does not present periodic boundary conditions. In fact a uniform electric field can be seen as the limit for $\mathbf{q} \to 0$ of a long wave-length field.

$$\lim_{\mathbf{q}\to 0} e\mathcal{E}\frac{e^{i\mathbf{q}\cdot\mathbf{r}}}{i\mathbf{q}\cdot\mathbf{r}} = e\mathcal{E}\mathbf{r}.$$

If we insert a long wave-length electric field into Eq. 3.27, perform a Taylor expansion in powers of $\mathbf{q}$ and take the limit $\mathbf{q} \to 0$, after some algebra we obtain

$$E^{(3)} = -i \sum_{k,v,v'} \langle u^{(0)}_{k,v}| \frac{\partial}{\partial k} \left(|u^{(0)}_{k,v'}\rangle\langle u^{(1)}_{k,v'}| \right) P_c |u^{(1)}_{k,v}\rangle$$

where u^0 and u^1 denote respectively the zero and first order correction to the periodic part of the Bloch function. This is the same formula obtained by Dal Corso and Mauri [54] in a different way.

Appendix D
Frozen Phonon Technique

In this appendix we discuss in some detail the frozen phonon technique used to obtain the coefficients of Tab. 3.1. The notations are the same as in Ref. [55]. B_{xyz} is obtained by frozen phonon technique considering optical displacements at Γ, the others using a double cell.

We consider optical phonons at the Brillouin zone center. For diamond-structure materials the displacements of atoms from the equilibrium position related to a zone center optical phonon is given by

$$\Delta\tau_s = (-1)^s u_\lambda$$

where s labels atomic sites ($s = 1, 2$) and λ ($\lambda = x, y, z$) labels Cartesian indices. Expanding the energy with respect to atomic displacements from equilibrium position

$$E_\Gamma(\mathbf{u}) = E_\Gamma^{(0)} + E_\Gamma^{(2)} + E_\Gamma^{(3)} + \cdots. \tag{D.1}$$

Here

$$E_\Gamma^{(2)} = M\omega_{LTO}^2(u_x^2 + u_y^2 + u_z^2) \tag{D.2}$$

$$E_\Gamma^{(3)} = B_{xyz}\, u_x u_y u_z \tag{D.3}$$

where M is the Silicon mass and ω the zone-center optical frequency.

From Eq. D.3 we note that taking a displacement in the [100] and [110] directions, the third order correction to the total energy vanishes. The frozen-phonon calculations are

Table D.1: Comparison of the second-order anharmonic coupling constants between phonons at the Γ and X points of the Brillouin zone in Silicon, as obtained by density-functional perturbation theory (DFPT) and the frozen-phonon (FP) method. Units are cm^{-1}.

	$\omega_{LTO}(\Gamma)$	$\omega_{TA}(X)$	$\omega_{LAO}(X)$	$\omega_{TO}(X)$
DFPT	518.95	157.11	412.65	458.89
FP	518.82	157.78	412.87	459.23

carried out by making a series of displacements along symmetry direction [111]; the two parameters are then obtained by fitting the results to this expression.

Calculations

The Brillouin-zone integration is performed using special point technique [37]. We have used the $(4,4,4)$ Monkhorst-Pack [32] integration mesh which, for the undistorted crystal, reduces to the 2-point Chadi-Cohen [37] set, while for the distorted geometry considered here, it gives 5 non equivalent points in the irreducible wedge of the Brillouin zone. The data where fitted with a third order polynomial and using the Least Square Method. The results are shown in Fig. D.1 The resulting frequency is reported in table D.1 and compared with that obtained through DFPT, showing excellent agreement.

Test at X

We have to consider a double cell along the z axis as that show in figure D.2. The phonons obtained at zone center of enlarged cell maps both the Γ point and the X point at $\frac{2\pi}{a}\hat{\mathbf{z}}$ (a is the lattice parameter). To eliminate the three translational degrees of freedom, we write the displacements of the atoms from equilibrium position

$$\mathbf{u}_1 = -\mathbf{u} + \mathbf{v} + \mathbf{w}$$

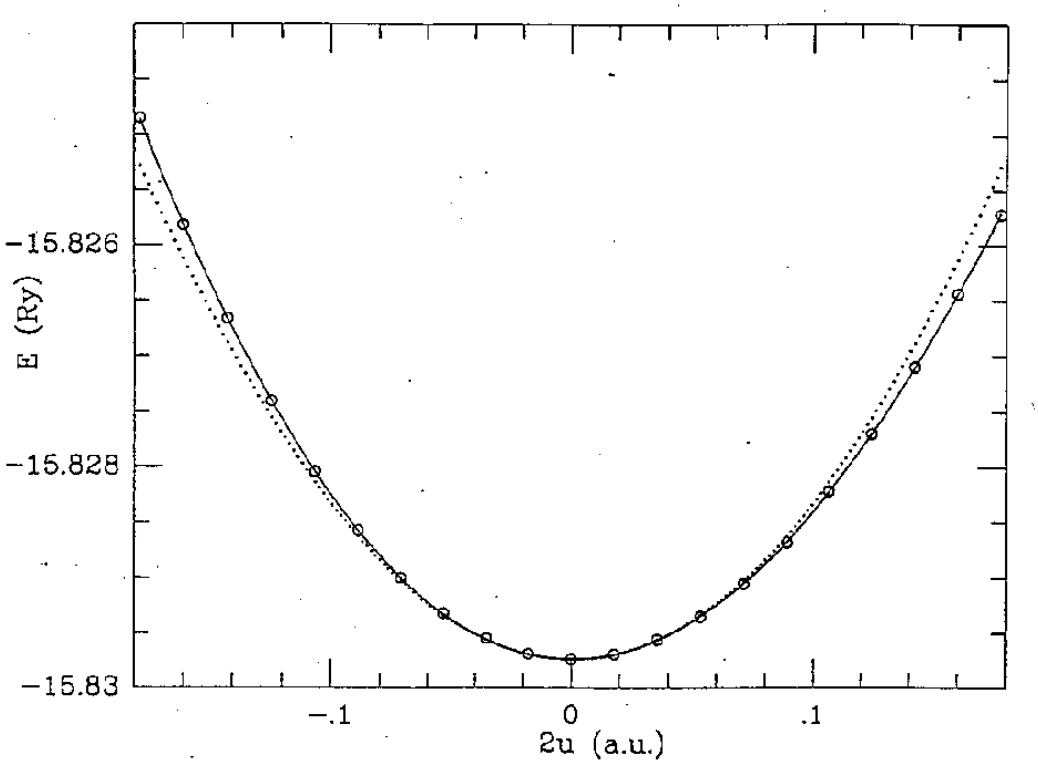

Figure D.1: Plot of the total energy (in Ry) per unit cell as a function of the relative displacement (in atomic units) of the two atoms along [111] direction; white circles are the values calculated using DFT; they are fitted by a third order polynomial (full line); the dotted line is the parabola obtained using second order coefficient from the fit.

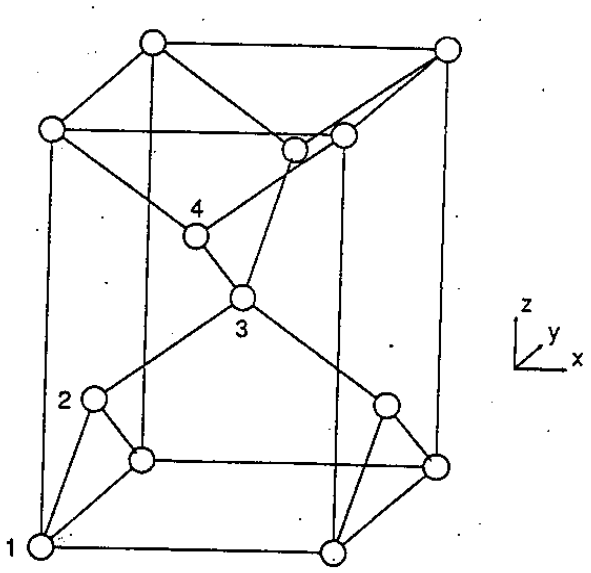

Figure D.2: Double cell used for the calculation of anharmonic coefficient at X-point

$$\mathbf{u}_2 = +\mathbf{u} + \mathbf{v} - \mathbf{w}$$

$$\mathbf{u}_3 = -\mathbf{u} - \mathbf{v} - \mathbf{w}$$

$$\mathbf{u}_4 = +\mathbf{u} - \mathbf{v} + \mathbf{w}$$

The energy referred to a cell of four atoms (double cell) is given by Eq (4.4)-(4.7) [55].

$$E_{tot} = E^{(0)} + E^{(2)} + E^{(3)} + ...$$

$$\begin{aligned} E^{(2)} &= 2E_\Gamma^{(2)} + 2M\omega_{TO}^2(X)(v_x^2 + w_y^2) + \\ &+ 2M\left[\omega_{TA}^2(X)(v_y^2 + w_x^2) + \omega_{LAO}^2(X)(v_z^2 + w_z^2)\right] \end{aligned} \tag{D.4}$$

$$\begin{aligned} E^{(3)} &= 2E_\Gamma^{(3)} + I_{zaa}u_z(v_x^2 - w_y^2) + I_{zbb}u_z(v_y^2 - w_x^2) + I_{zcc}u_z(v_z^2 - w_z^2) \\ &+ I_{zac}(u_x v_x v_z - u_y w_y w_z) + I_{ybc}(u_y v_y v_z - u_x w_x w_z) \end{aligned} \tag{D.5}$$

Now to compute the five third order coefficients we have to move the atoms along five different directions, in analogy with what we have done for the simple cell.

Computation of $\mathbf{I}_{zaa}$
Displacement I:

$$\mathbf{u} = t\hat{\mathbf{z}}; \quad \mathbf{v} = t\hat{\mathbf{x}}; \quad \mathbf{w} = 0.$$

The energy becomes:

$$E_{tot} = E^{(0)} + 2M\omega_{LTO}^2(\Gamma)t^2 + 2M\omega_{TO}^2(X)t^2 + I_{zaa}t^3;$$

in the distorted geometry we have 4 k-point Chadi-Cohen set in the irreducible wedge.

Computation of $\mathbf{I}_{zbb}$
Displacement II:

$$\mathbf{u} = t\hat{\mathbf{z}}; \quad \mathbf{v} = t\hat{\mathbf{y}}; \quad \mathbf{w} = 0.$$

The energy becomes:

$$E_{tot} = E^{(0)} + 2M\omega_{LTO}^2(\Gamma)t^2 + 2M\omega_{TA}^2(X)t^2 + I_{zbb}t^3$$

in the distorted geometry we have 4 k-points in the irreducible wedge.

Computation of $\mathbf{I}_{zcc}$

Displacement III:

$$\mathbf{u} = t\hat{\mathbf{z}}; \quad \mathbf{v} = t\hat{\mathbf{z}}; \quad \mathbf{w} = 0.$$

The energy becomes:

$$E_{tot} = E^{(0)} + 2M\omega_{LTO}^2(\Gamma)t^2 + 2M\omega_{LAO}^2(X)t^2 + I_{zcc}t^3$$

in the distorted geometry we have 4 k-points in the irreducible wedge.

Computation of $\mathbf{I}_{xac}$

Displacement IV:

$$\mathbf{u} = t\hat{\mathbf{x}}; \quad \mathbf{v} = t\hat{\mathbf{x}} + t\hat{\mathbf{z}}; \quad \mathbf{w} = 0.$$

The energy becomes:

$$E_{tot} = E^{(0)} + 2M\omega_{LTO}^2(\Gamma)t^2 + 2M\omega_{TO}^2(X)t^2 + 2M\omega_{LAO}^2(X)t^2 + I_{xac}t^3$$

in the distorted geometry we have 6 k-points in the irreducible wedge.

Computation of $\mathbf{I}_{ybc}$

Displacement V:

$$\mathbf{u} = t\hat{\mathbf{y}}; \quad \mathbf{v} = t\hat{\mathbf{y}} + t\hat{\mathbf{z}}; \quad \mathbf{w} = 0.$$

The energy becomes:

$$E_{tot} = E^{(0)} + 2M\omega_{LTO}^2(\Gamma)t^2 + 2M\omega_{TA}^2(X)t^2 + 2M\omega_{LAO}^2(X)t^2 + I_{ybc}t^3$$

in the distorted geometry we have 6 k-points in the irreducible wedge.

Using a polynomial fit and the values of B_{xyz} obtained previously we can extract the third order coefficient reported in 3.1. The frequencies at X reported in table D.1 are obtained computing the second order coefficient of displacements I,II and III and then subtracting the frequency $\omega_{LTO}(\Gamma)$. As a further test we have also computed the second order coefficients along direction IV and V and compared which those obtained with the frequencies of tab D.1 (fit along I,II and III direction); the relative error is less than $3.10^{-4}\%$.

Appendix E
Ionic term

The ionic term in the anharmonic force constants arises from the ion-ion Ewald contribution [56]:

$$E_{Ewald} = \frac{4\pi N}{\Omega}\frac{e^2}{2}\left[\sum_{(\mathbf{G}\neq 0)}\frac{e^{-G^2/4\eta}}{G^2}\left|\sum_l Z_l e^{i\mathbf{G}\cdot\tau_l}\right| - \frac{1}{4\eta}\left(\sum_l Z_l\right)^2\right]$$
$$+\frac{Ne^2}{2}\sum_{l,m}\sum_R \frac{Z_l Z_m}{|\tau_l - \tau_m - \mathbf{R}|}\left[1 - erf\left(\sqrt{\eta}|\tau_l - \tau_m - \mathbf{R}|\right)\right]$$
$$-Ne^2\left[\frac{\eta}{\pi}\right]^{\frac{1}{2}}\sum_l Z_l^2$$

where Z_i indicates the bare ionic (pseudo)charge for the ith atom, Ω is volume of the unit cell, η is an arbitrary parameter, it may be chosen so large to allow to neglect the real-space term. After some straightforward algebra we find for the ionic contribution to the third order anharmonic constant

$$\tilde{E}^{ion}_{ss's'',\alpha\beta\gamma}(\mathbf{q}_1,\mathbf{q}_2,\mathbf{q}_3) =$$
$$= -\frac{2\pi e^2 N}{3\Omega}\sum_{(\mathbf{G}\neq 0)}\frac{e^{-G^2/4\eta}}{G^2}G_\alpha G_\beta G_\gamma Z_s\left[\sum_{\tilde{s}} Z_{\tilde{s}}\sin\mathbf{G}\cdot(\tau_{\tilde{s}} - \tau_s)\right]\delta_{s,s'}\delta_{s',s''}$$
$$+\frac{2\pi e^2}{\Omega}\sum_{(\mathbf{G}\neq 0)}\frac{e^{-(\mathbf{q}_2+\mathbf{q}_3+\mathbf{G})^2/4\eta}}{G^2}(q_{2,\alpha}+q_{3,\alpha}+G_\alpha)(q_{2,\beta}+q_{3,\beta}+G_\beta)$$
$$\times(q_{2,\gamma}+q_{3,\gamma}+G_\gamma)Z_s Z_{s'}\sin\mathbf{G}\cdot(\tau_s - \tau_{s'})\delta_{s',s''} \qquad \text{(E.1)}$$

Appendix F
Convergence tests

In this appendix we illustrate the convergence test performed for germanium in order to examine the accuracy of our calculations (similar test are performed for silicon and diamond). In Tab. F.1 we show how some third order anharmonic coefficients change with increasing cutoff (*i.e.* the number of plane waves in the basis set). In our computation we have used a kinetic energy cutoff of $22Ry$.

In Tab. F.2 we show some anharmonic coupling constants computed with the mesh used in our computation (the 10-points Chadi-Cohen [37] set in the irreducible wedge), are compared with those obtained with a larger mesh.

We estimate that the overall numerical accuracy of our calculations is of few percent.

Table F.1: Convergence test for Ge, 10 Chadi and Cohen k-points, a=10.60 a.u.

cutoff (Ry)	B_{xyz}	$I_{z\overline{aa}}$	$I_{z\overline{bb}}$	$I_{z\overline{cc}}$	$I_{\overline{xac}}$	$I_{\overline{ybc}}$
16	-239.53	200.58	-36.35	46.27	374.86	-57.74
20	-239.01	200.81	-35.70	48.99	375.46	-56.73
22	-236.25	198.41	-35.27	48.23	370.73	-56.01
24	-234.45	196.63	-35.25	47.36	367.15	-55.94
28	-233.25	195.47	-35.42	46.60	364.72	-56.13

Table F.2: Convergence test for Ge for Chadi and Cohen k-points, a=10.60 a.u., kinetic energy cutoff of 22 Ry.

k-point	B_{xyz}	$I_{z\overline{aa}}$	$I_{z\overline{bb}}$	$I_{z\overline{cc}}$	$I_{\overline{xac}}$	$I_{\overline{ybc}}$
10	-236.25	198.41	-35.27	48.23	370.73	-56.01
28	-234.64	197.19	-35.34	47.28	371.15	-56.26

Appendix G
Structural properties at equilibrium

In this appendix we present some details of the preliminary structural and lattice-dynamical properties which provide the input of our study. The crystal equilibrium structure is determined by minimizing the total energy functional *vs.* the lattice parameter. We fixed the kinetic energy cutoff (*i.e.* the square modulus of all the plane waves is less than a fixed value G_{MAX} related to the kinetic energy cutoff by $E_{cut} = \frac{\hbar^2 G_{MAX}^2}{2m}$ where m is the electron mass) and compute the total energy per unit cell at different volumes. This correspond to fixing the real space resolution *i.e.* the distance between the points of a real space grid. The number of point used changes when the volume is changed. In this way we have a different number of plane waves for different volumes; since the Monkhorst-Pack mesh is discrete, we can have some small discontinuity in the values of the total energy changing the crystal volume. We avoid this problem by fitting the total energy to an appropriate equation of state.

To determine the equilibrium lattice constant we compute the total energy for different values of the volume Ω. The data obtained are fitted to a Murnaghan's equation of state [57]:

$$E = \frac{\Omega_0 B_0}{B_0'}\left[\frac{1}{B_0'-1}\left(\frac{\Omega}{\Omega_0}\right)^{B_0'-1} + \frac{\Omega}{\Omega_0}\right] + const., \qquad \text{(G.1)}$$

where B_0 is the bulk modulus, B_0' the derivative of B_0 with respect to pressure and Ω_0 the

Table G.1: Equilibrium lattice parameter a (a.u.) used in the present calculation and the bulk modulus B_0 (Kbar). Parenthesis denote experimental data.

	C	Si	Ge
a	6.68	10.21	10.57
	(6.74)	(10.26)	(10.68)
B_0	4547	934	770
	(4420)	(978)	(758)

equilibrium volume of the crystal. The lattice parameter and the bulk modulus obtained in this way are in Tab. G.1

Deriving the Murnaghan's energy equation with respect the volume, we obtain the equation of the pressure

$$P = \frac{B_0}{B_0'}\left[\left(\frac{\Omega_0}{\Omega}\right)^{B_0'} - 1\right] \tag{G.2}$$

The results on pressure dependence were obtained by computing the linewidth at a given volume; the corresponding pressure was found through Eq. G.2. In Tab. G.1 we show the lattice constant and the bulk modulus obtained in this way.

In the remaining part of this appendix we report some results for phonon frequencies. This data where obtained with the same k-mesh and kinetic energy cutoff as the results shown in Cap. 4. We have seen in Eq. 2.8 that to compute the linewidth we have to perform an integration over the constant energy surface of the phonon frequencies, so it is necessary to reproduce accurately the phonon branches. The values reported in Tab. G.2 for some high symmetry points reproduce those of [21] and are in excellent agreement with experimental data.

Finally, in Tab. G.3 we report the values obtained for the third-order anharmonic constants in order to compare the dynamical tensor of different materials.

Table G.2: Phonon frequencies computed at high-symmetry points, Γ X and L (in units of cm^{-1}). Parenthesis denote experimental data.

	Γ	X_{TA}	X_{TO}	X_{LAO}	L_{TA}	L_{LA}	L_{TO}	L_{LO}
C	1316	793	1088	1217	553	1070	1223	1265
	(1331)	(803)	(1077)	(1194)	(552)	(1035)	(1210)	(1242)
Si	509	141	455	406	107	372	485	408
	(517)	(150)	(463)	(410)	(114)	(378)	(487)	(417)
Ge	301	82	272	241	63	224	243	288
	(304)	(80)	(276)	(241)	(63)	(222)	(245)	(290)

Table G.3: Comparison of the third-order anharmonic coupling constants between phonons at the Γ and X points of the Brillouin zone in Diamond, Silicon and Germanium, as obtained by density-functional perturbation theory (DFPT). Same notation as in section 3.4.3. Units are eV/Å^3.

	B_{xyz}	$I_{z\overline{aa}}$	$I_{z\overline{bb}}$	$I_{z\overline{cc}}$	$I_{\overline{xac}}$	$I_{\overline{ybc}}$
C	-991.79	782.50	-61.67	310.16	1445.47	-151.40
Si	-284.25	227.37	-37.64	49.91	441.32	-63.91
Ge	-242.81	203.69	-36.14	48.39	381.10	-57.63

Appendix H
Phenomenological theory

In this appendix we summarize the phenomenological theory to explain the splitting between TO-LO branches at the Brillouin zone center. In a polar crystal the longitudinal phonon at $\mathbf{q} = 0$ induces a change in the dipole moment producing an electric field. The coupling of the electric field with the phonon produce an additional non analytical contribution in the dynamical matrix, which gives the TO-LO splitting. In this case the internal energy depends on the phonons displacements and a long-wave electric field $\vec{\mathcal{E}}$. Expanding up to the second order we have

$$\begin{aligned} E &= \sum_{\mathbf{q}} \left[\sum_{s,s';\alpha\beta} C_{s,s',\alpha\beta}(\mathbf{q}) u_{\alpha,s}(\mathbf{q}) u_{\beta,s'}(\mathbf{q}) \right. \\ &- \left. \sum_{s,\alpha,\beta} e Z_s^{*\alpha,\beta} u_{\alpha,s}(\mathbf{q}) \mathcal{E}_\beta(\mathbf{q}) - \frac{\Omega}{8\pi} \sum_{\alpha\beta} \epsilon_\infty^{\alpha\beta} \mathcal{E}_\alpha(\mathbf{q}) \mathcal{E}_\beta(\mathbf{q}) \right] \end{aligned} \tag{H.1}$$

where Z_s^* is the effective charge tensor, $-e$ the electron charge, Ω the unit cell volume and ϵ_∞ the hight-frequency (electronic) dielectric tensor. The force acting on an ion is given by

$$F_{s,\alpha}(\mathbf{q}) = -\frac{\partial E}{\partial u_{\alpha,s}(\mathbf{q})} = -\sum_{\beta} \left[\sum_{s'} C_{s,s',\alpha\beta}(\mathbf{q}) u_{\beta,s'}(\mathbf{q}) - e Z_s^{*\alpha,\beta} \mathcal{E}_\beta(\mathbf{q}) \right] \tag{H.2}$$

The displacement field is

$$\mathcal{D}_\alpha = -\frac{1}{\Omega} \frac{\partial E}{\partial \mathcal{E}_\alpha}$$

From electrostatics we have

$$\mathrm{div}\vec{\mathcal{D}} = \vec{\mathcal{D}} \cdot \mathbf{q} = 0 \tag{H.3}$$

and

$$\mathrm{curl}\vec{\mathcal{E}} = \vec{\mathcal{E}} \wedge \mathbf{q} = 0; \quad \Longrightarrow \vec{\mathcal{E}} = \hat{\mathbf{q}} \cdot (\hat{\mathbf{q}} \cdot \vec{\mathcal{E}}) \tag{H.4}$$

where $\hat{\mathbf{q}}$ is the versor along the $\mathbf{q}$ direction. From Eq. H.2 we obtain

$$\vec{\mathcal{E}} = -\frac{4\pi e}{\Omega} \sum_{s'} \frac{\hat{\mathbf{q}}(\sum_{\alpha',\beta'} \hat{q}_{\alpha'} Z_{s'}^{*\alpha',\beta'} u_{s',\beta'}(\mathbf{q}))}{\hat{\mathbf{q}} \cdot \epsilon_\infty \cdot \hat{\mathbf{q}}} \tag{H.5}$$

Substituting this expression in Eq. H.2 we finally obtain

$$C_{s,s',\alpha\beta}^{non\ an.}(\mathbf{q}) = C_{s,s',\alpha\beta}(\mathbf{q}) + \frac{4\pi e^2}{\Omega} \frac{(\sum_{\alpha'} Z_s^{*\alpha,\alpha'} \hat{q}_{\alpha'})(\sum_{\beta'} Z_{s'}^{*\beta,\beta'} \hat{q}_{\beta'})}{\hat{\mathbf{q}} \cdot \epsilon_\infty \cdot \hat{\mathbf{q}}} \tag{H.6}$$

This treatment is valid when the electric field is slowly varying in space ($\mathbf{q} \sim 0$). The non analytical behavior of the dynamical matrix is explicitly shown by the second term on the rhs of Eq. H.6 since it depends of the orientation of $\mathbf{q}$.

As an example, we consider the case of GaAs. The effective charge tensor is diagonal $Z_s^{*\alpha,\beta} = Z_s^* \delta_{\alpha,\beta}$ and the translational invariance imply $Z_{Ga}^* = -Z_{As}^* = Z^*$. Specializing Eq. H.6, we obtain that the frequency of the longitudinal optical phonon is

$$\omega_{LO} = \sqrt{\omega_{TO} + \frac{4\pi e^2}{\Omega} \frac{Z^{*2}}{\mu \epsilon_\infty}}$$

Where $\mu = \frac{M_{Ga} M_{As}}{M_{Ga} + M_{As}}$ is the reduced mass of the system.

Acknowledgements

I would like to thank my supervisor Stefano Baroni for introducing me to the field of the electronic structure calculations and for the encouragement throughout this thesis. Thanks also to Elisa Molinari for a critical reading of this thesis and for many helpful discussions. Part of this work is the result of a fruitful collaboration with her. As special thank is due to Raffaele Resta and Stefano De Gironcoli for continuous help and advice. I am grateful to Manuel Cardona for his interest in this work and for several suggestions he gave me.

During my stay at SISSA I took advantage from many scientific and non scientific conversation with my colleague graduate students, previous graduate student and post-docs: Marco Airoldi, Marco Bernasconi, Claudia Bungaro, Andrea Dal Corso, Franz Di Tolla, Andrea Ferrante, Alberto Franceschetti, Nicola Manini, Pasquale Pavone, Santi Prestipino, Sandro Scandolo, Kurt Stokbro and Riccardo Valente.

A particular thank to the computer staff: Marina Picek, Luisa Urgias, Roberto Innocente and Fabio Lonzar for its kindness and efficiency.

Finally I want to thank Giovanna, Fabrizio, Marilena and all the friends who made more agreeable my stay in Trieste.

Bibliography

[1] For a review see: J.A. Kash and J.C. Tsang, in *Light Scattering in Solids VI*, edited by M. Cardona and G. Güntherodt (Springer, Berlin, 1991), p. 423.

[2] J. Menéndez and M. Cardona, Phys. Rev. B **29**, 2051 (1984).

[3] For a review see: M. Cardona et al., J. Phys.: Condens. Matter **5**, A61 (1993).

[4] P.A.Temple and C.E.Hathaway, Phys Rev. B, **7**, 3685 (1973).

[5] Handbook of chemistry and physics, 1993-1994 74-th edition, edited by D. R. Lide, CRC Press, Inc.

[6] H.D.Fuchs, C.H.Grein, R.I.Devlen, J.Kuhl and M. Cardona, Phys. Rev. B **44**, 8633 (1991).

[7] W. E. Bron, J. Kuhl and B. K. Rhee, Phys. Rev. B **34**, 6961 (1986).

[8] J. Kuhl and W. E. Bron, Solid State Commun. **49**, 935 (1984).

[9] D. von der Linde, J. Kuhl and H. Klingenberg, Phys. Rev. Lett. **23**, 1505 (1980).

[10] R.A. Cowley, J. Phys. (Paris) **26**, 659 (1965).

[11] P.G. Klemens, Phys. Rev. **148**, 845 (1966).

[12] S. Narasimhan and D. Vanderbilt, Phys. Rev. B **43**, 4541 (1991).

[13] *(a)* R.S. Krishnan, Proc. Indian Acad. Sci. **24**, 45 (1946); *(b)* S.A. Solin and A.K. Ramdas, Phys. Rev. B **1**, 1687 (1970); *(c)* E. Anastassakis, H.C. Hwang, and C.H. Perry, Phys. Rev. B **4**, 2493 (1971); *(d)* W.J. Borer, S.S. Mitra, and K.W. Namjoshi, Solid State Commun. **9**, 1377 (1971); *(e)* R.M. Chrenko, J. Appl. Phys. **63**, 5873 (1988); *(f)* M.A. Washington and H.Z. Cummins, Phys. Rev. B **15**, 5840 (1977); *(g)* K.C. Hass et al., Phys. Rev. B **44**, 12046 (1991); *(h)* J. Spitzer et al., Solid State Commun. **88**, 509 (1993).

[14] S. Usher and G. P. Srivastava, Phys. Rev. B, **50**, 14179 (1994).

[15] Landoldt Börnstein, Numerical Data and Functional Relationship in Science and Technology, New series, **17**a, ed. by O. Madelung (New York 1982).

[16] S. Baroni, P. Giannozzi and A. Testa, Phys. Rev. Lett. **58**, 1861 (1987).

[17] X. Gonze and J. P. Vigneron, Phys. Rev. B **39**, 13120 (1989).

[18] P. Giannozzi, S. de Gironcoli, P. Pavone and S. Baroni, Phys. Rev. B **43**, 7231 (1991).

[19] S. Baroni, P. Giannozzi, and A. Testa, Phys. Rev. Lett. **59**, 2662 (1987).

[20] S. de Gironcoli, S. Baroni, and R. Resta, Phys. Rev. Lett. **62**, 2843 (1989); S. de Gironcoli, S. Baroni, and R. Resta, Ferroelectrics, **111**, 19 (1990); A. Dal Corso, R. Resta, and S. Baroni, Phys. Rev. B **47**, 16252 (1993); A. Dal Corso, S. Baroni, and R. Resta, Phys. Rev. B **49**, 5323 (1994).

[21] P. Giannozzi, S. de Gironcoli, P. Pavone, and S. Baroni, Phys. Rev. B **43**, 7231 (1991).

[22] F. Ancilotto, A. Selloni, W. Andreoni, S. Baroni, R. Car, and M. Parrinello, Phys. Rev. B **43**, 8930, (1991); X. Gonze, D. C. Allan, and M. P. Teter, Phys. Rev. Lett. **68**, 3603, (1992); M. Buongiorno Nardelli, S. Baroni, and P. Giannozzi, Phys. Rev. Lett. **69**, 1069, (1992); A. Dal Corso, S. Baroni, R. Resta, and S. de Gironcoli, Phys. Rev. B **47**, 3588, (1993); P. Pavone, K. Karch, O. Schütt, D. Strauch, P. Giannozzi, and S. Baroni, Phys. Rev. B **48**, 3156, (1993); J. Fritsch, P. Pavone, and U. Schröder, Phys. Rev. Lett. **71**, 4194, (1993); C. Lee and X. Gonze, Phys. Rev. Lett. **72**, 1686,

(1994); C.-Z. Wang, R. Yu, and H. Krakauer, Phys. Rev. Lett. **72**, 368, (1994); S .Y. Savranov, D. Y. Svranov, and O. K. Andersen, Phys. Rev. Lett. **72**, 372, (1994); P. Giannozzi and S. Baroni, J. Chem. Phys. **100**, 8537 (1994).

[23] See for instance P. M. Morse and H. Feshbach, *Methods of Theoretical Physics* (Mc Graw-Hill, New York, 1953), Vol. II, P. 1120.

[24] T. S. Nee, R. G. Parr and R. J. Bartlett, J. Chem. Phys. **64**, 2216 (1976).

[25] S. de Gironcoli, P. Giannozzi, and S. Baroni, Phys. Rev. Lett. **66**, 2196 (1991); N. Marzari, S. de Gironcoli, and S. Baroni, Phys. Rev. Lett. **72**, 4011 (1994).

[26] S. Baroni, M. Peressi, R. Resta, and A. Baldereschi, Proc. 21^{st} Intl. Conf. on *The Physics of Semiconductors*, edited by P. Jiang and Hou-Zhi Zheng (World-Scientific, Singapore, 1993), p. 863; M. Peressi and S. Baroni, Phys. Rev. B **49**, 7490 (1994).

[27] P. Hohenberg and W. Kohn, Phys. Rev. **136**, **B**864 (1964).

[28] AA.VV., *Theory of the inhomogeneous electron gas*, edited by S. Lundquist and N. H. March (Plenum, New York, 1983).

[29] W. Kohn and L. J. Sham, Phys. Rev. A **140**, 1133 (1965).

[30] L. I. Schiff, *Quantum Mechanics*, Mc Graw-Hill, Inc. (Singapore 1986).

[31] A. Debernardi and S. Baroni, Solid State Commun. **91**, 813 (1994).

[32] H.J. Monkhorst and J.D. Pack, Phys. Rev. B **13**, 5188 (1976).

[33] D. Vanderbilt S. H. Taole and S. Narasimhan, Phys. Rev. B **40**, 5657 (1989); Errata: *ibid.* **42**, 11373 (1990).

[34] D.M. Ceperley and B.J. Alder, Phys. Rev. Lett. **45**, 566 (1980).

[35] J. Perdew and A. Zunger, Phys. Rev. B **23**,5048 (1981).

[36] U. von Barth and R.Car, unpublished.

[37] A. Baldereschi, Phys Rev.B **7**, 5212 (1973); D.J. Chadi and M.L. Cohen, Phys Rev.B **8**, 5747 (1973); D.J. Chadi, Phys. Rev. B **16**, 1746 (1977).

[38] G. Lehman and M. Taut, Phys. Status Solidi B **54**, 469 (1972).

[39] O. Jepsen and O.K. Andersen, Solid State Commun. **9**, 1763 (1971).

[40] P. Giannozzi et al., Phys. Rev. B **43**, 7231 (1991).

[41] Preliminary results were reported in A. Debernardi, S. Baroni, and E. Molinari, in *Proc. of the 22nd International Conference on the Physics of Semiconductors*, edited by D.J. Lockwood (World Scientific, Singapore, 1994), p. 373. The present data are obtained with an improved convergence in the plane wave expansion.

[42] A. Debernardi, S. Baroni and E. Molinari, Phys. Rev. Lett. **75**, 1819 (1995).

[43] *(a)* T.R. Hart, R.L. Aggarwal, and B. Lax, Phys. Rev. B **1**, 638 (1970); *(b)* R. Tubino, L. Piseri, and G. Zerbi, J. Chem. Phys. **56**, 1022 (1972); *(c)* P.A. Temple and C.E. Hathaway, Phys. Rev. B **7**, 3685 (1973); *(d)* M. Balkanski, R.F. Wallis, and E. Haro, Phys. Rev. B **28**, 1928 (1983); *(e)* Ref. [2].

[44] *(a)* R.K. Ray, R.L. Aggarwal, and B. Lax, in *Light Scattering in Solids*, edited by M. Balkanski (Flammarion, Paris, 1971), p. 288; *(b)* F. Cerdeira and M. Cardona, Phys. Rev. B **5**, 1440 (1972); *(c)* Ref. [2]; *(d)* H.D. Fuchs et al., Phys. Rev. B **44**, 8633 (1991).

[45] P. Pavone et al., Phys. Rev. B **48**, 3156 (1993).

[46] Bernard A. Weinstein and G. J. Piermarini, Phys. Rev.B **12**, 1172 (1975).

[47] See, for example, R. Resta, *Proprietés diélectriques des matériaux et dynamique du réseau: Etat présent de la théorie ab-initio*, unpublished; and AA.VV., *Theory of lattice dynamics in the harmonic approximation*, edited by H. Ehrenreich, F. Seitz and D. Turnbull (Academic Press, New York, 1971).

[48] W. Cochran and R. A. Cowley, J.Phys.Chem.Solids **23**, 447 (1962).

[49] R. M. Pick, M. H. Cohen and R. M. Martin, Phys. Rev. B , **1** 910 (1970).

[50] R. Resta, Phys. Rev. B **27**, 3620 (1983).

[51] For a review of DFT see, for example, R. Resta, *SISSA lecture notes*, unpublished; and AA.VV., *Theory of the Inhomogeneous Electron Gas*, edited by S. Lundquist and N.H. March (Plenum, New York, 1983).

[52] B. Kh. Bairamov, Yu. É. Kitaev, V. K. Negoduiko and Z. M. Khashkhozhev, Fiz. Tverd. Tela (Leningrad) **16**, 2036 (1974) [Sov.Phys.–Solid State **16**, 1323 (1975)].

[53] F. Vallée and F. Bogani, Phys. Rev. B **43**, 12 049 (1991).

[54] A. Dal Corso and F. Mauri, Phys. Rev. B **50**, 5756 (1994).

[55] D. Vanderbilt, S.H. Taole and S. Narasimhan, Phys Rev.B **40**, 5657 (1989).

[56] M.T. Yin and M.L. Cohen, Phys. Rev.B **26**, 3259 (1982).

[57] F. D. Murnaghan, Proc. Nat. Acad. Sci. USA, **50**, 697 (1973).